ELSEVIER

Journal of Hepatology 43 (2005) 757–763

Journal of Hepatology

www.elsevier.com/locate/jhep

Hepatitis C virus core protein exerts an inhibitory effect on suppressor of cytokine signaling *(SOCS)-1* gene expression

Hideyuki Miyoshi[1], Hajime Fujie[1], Yoshizumi Shintani[1], Takeya Tsutsumi[1], Seiko Shinzawa[1], Masatoshi Makuuchi[2], Norihiro Kokudo[2], Yoshiharu Matsuura[3], Tetsuro Suzuki[4], Tatsuo Miyamura[4], Kyoji Moriya[1], Kazuhiko Koike[1,*]

[1]*Department of Internal Medicine, Graduate School of Medicine, University of Tokyo, Tokyo, Japan*
[2]*Department of Hepatobiliary, Pancreatic and Transplantation Surgery, Graduate School of Medicine, University of Tokyo, Tokyo, Japan*
[3]*Research Center for Emerging Infectious Diseases, Research Institute for Microbial Diseases, Osaka University, Osaka, Japan*
[4]*Department of Virology II, National Institute of Infectious Diseases, Tokyo, Japan*

***Background/Aims*: Suppressor of cytokine signaling (SOCS)-1, a negative feedback regulator of cytokine signaling pathway, also has a tumor suppressor activity, the silencing of its gene by hypermethylation is suggested to contribute to hepatocarcinogenesis. We studied the effect of the core protein of hepatitis C virus (HCV) on the expression of *SOCS-1* gene.**

***Methods*: HCV core gene transgenic mice, which develop hepatocellular carcinoma late in life, HepG2 cells expressing the core protein, and human liver tissues were analyzed.**

***Results*: The expression of *SOCS-1* gene was significantly suppressed in the liver of core gene transgenic mice and HepG2 cells expressing the core protein, while that of *SOCS-3* gene was conserved. *SOCS-1* expression levels also decreased in HCV-positive human liver tissues. The core protein differentially down-regulated the expression of signal transducer and activator of transcription (STAT) target genes, but rather enhanced STAT1 and STAT3 activation after interleukin-6 stimulation in mouse liver tissues and cells.**

***Conclusions*: HCV core protein down-regulates the expression of *SOCS-1* gene. This is a mechanism leading to *SOCS-1* silencing, an alternative to the hypermethylation of the gene; this effect of the core protein may modulate the intracellular signaling pathway, contributing to the pathogenesis in HCV infection including hepatocarcinogenesis.**

***Keywords*: Tumor suppressor gene; Hepatocellular carcinoma; Transgenic mouse; STAT3**

1. Introduction

Hepatitis C virus (HCV) infection is a major cause of chronic hepatitis. A substantial proportion of patients with chronic hepatitis C eventually develop hepatocellular carcinoma (HCC), which is one of the leading causes of death worldwide [1,2]. Despite the absence of appropriate in vitro replication systems or practical infectious animal model systems, the mechanism underlying hepatocarcinogenesis in human HCV infection is gradually clarified. Both the direct and indirect effects of HCV on HCC development are demonstrated [3–6]. The accumulation of gene aberrations, such as the inactivation of tumor suppressor genes or the activation of oncogenes, which are induced through the inflammation-mediated continuous death of hepatocytes followed by regeneration, may be one of the mechanisms underlying hepatocarcinogenesis [3]. On the other hand, the viral gene products are suggested to contribute to the development of HCC by their direct effects on hepatocytes [4]. Such direct effects have been demonstrated by the use of model systems including mice

Received 17 September 2004; received in revised form 11 March 2005; accepted 16 March 2005; available online 31 May 2005

* Corresponding author. Address: Department of Infectious Diseases, Internal Medicine, Graduate School of Medicine, University of Tokyo, 7-3-1 Hongo, Bunkyo-ku, Tokyo 113-8655, Japan. Tel.: +81 3 5800 8801; fax: +81 3 5800 8807.

E-mail address: kkoike-tky@umin.ac.jp (K. Koike).

0168-8278/$30.00
doi:10.1016/j.jhep.2005.03.028

[7–9]. HCV-infected hepatocytes produce viral structural and nonstructural proteins. Some of these confer certain phenotypes to hepatocytes and may be associated with the pathogenesis of HCV infection including the development of HCC. Among such viral proteins, the core protein of HCV has a variety of biological activities, including oncogenic activity, which substantially affects host cellular functions [7–11].

Suppressor of cytokine signaling (SOCS)-1, also called signal transducer and activator of transcription (STAT)-induced STAT inhibitor-1 or Jak binding protein-1, is a negative feedback regulator of cytokine signaling through the Jak/STAT pathway. SOCS-1 contains the SH2 domain and directly interacts with the kinase domain of Jak to suppress Jak activity. *SOCS-1* gene expression is augmented by various cytokines, such as interferon (IFN)-γ, interleukin (IL)-6 or leukemia inhibitory factor (LIF), resulting in the suppression of the signal transduction downstream pathways of these cytokines [12–14]. Moreover, SOCS-1 has been recently shown to exhibit a tumor suppressor activity. SOCS-1 suppresses the expression of several oncogenes or growth-related genes acting as a negative regulator of cell proliferation: the loss of function of SOCS-1 facilitates tumor progression [15–17]. As a mechanism underlying the loss of function of SOCS-1, a recent study has revealed a frequent silencing of the *SOCS-1* gene by CpG methylation in HCC tissues [18–20]. Alternatively, however, it may be possible that HCV infection, particularly, the proteins that the HCV genome encodes per se, may render the *SOCS-1* gene unable to exhibit its function by gene silencing.

We examined such a possibility using a mouse model for HCV infection that is destined to develop HCC [7,9], as well as cultured cells expressing the HCV core protein [21]. The core protein markedly suppressed the expression of the *SOCS-1* gene in both liver tissues and cultured cells. This silencing of the *SOCS-1* gene may be one of explanations for the pathogenicity of HCV in humans.

2. Materials and methods

2.1. Transgenic mouse and cell lines

HCV core gene transgenic mice have been described previously [7]. These mice develop HCC late in life [7,9]. The mice were cared for according to the institutional guidelines and maintained in a specific pathogen-free state. All the animals received humane care and the study protocol complied with the institution's guidelines for the care and use of experimental animals. HepG2 cell lines expressing the HCV core protein under the control of CAG promoter (Hep39J, Hep396 and Hep397) or a control HepG2 line (Hepswx) carrying the empty vector were described previously [21,22].

2.2. IL-6 Stimulation

For the in vivo experiments, 0.05–0.5 μg/g BW murine IL-6 (Diaclone, Besançon, France) was administered into 8 w.o. male mice i.p., and liver tissues were obtained 60 min later. Cultured cells were treated with human IL-6 (Diaclone) at 10–100 ng/ml or IFN-α at 1.0–10.0 ng/ml and then were harvested 60 min later.

2.3. Reverse transcription (RT)-PCR analysis

Total RNA was extracted from liver tissues or cultured cells before and after the treatment with IL-6 using TRIzol (Invitrogen). RNA was reverse-transcribed using oligo(dT) primers and Superscript II (Invitrogen). Equal amounts of cDNA were then subjected to PCR. The primer pairs used were:

5′-CACTCACTTCCGCACCTTCC-3′ (forward) and
5′-TCCAGCAGCTCGAAAAGGCA-3′ (reverse) for murine *SOCS-1*,
5′-CACGCACTTCCGCACATTCC-3′ (forward) and
5′-TCCAGCAGCTCGAAGAGGCA-3′ (reverse) for human *SOCS-1*,
5′-TCACCCACAGCAAGTTTCCCGC-3′ (forward) and
5′-GTTGACAGTCTTCCGACAAAGATGC-3′ (reverse) for murine *SOCS-3*,
5′-CACGCACTTCCGCACATTCC-3′ (forward), and
5′-GTTGACGGTCTTCCGACAGAGATGC-3′ (reverse) for human *SOCS-3*.

For the RT-PCR analysis, the quantity of cDNA template and the number of amplification cycles were optimized to ensure that the reaction was terminated during the linear phase of product amplification, so that the semiquantitative comparison of mRNA abundance between different samples was possible [23]. The intensities of the bands were determined using a densitometer. RT-PCR was also done using GAPDH primers to adjust the amounts of RNA in each experiment.

2.4. Human liver tissue samples and real-time PCR

Nine patients with HCC who had underlying chronic hepatitis C were studied for *SOCS-1* expression in noncancerous tissues. Additional nine patients, who were found to be negative for both HBsAg and anti-HCV at the time of operation, were also studied. The latter patients underwent liver resection for metastatic liver tumors from colon cancer. The experimental protocol conformed to the ethical guidelines of the 1975 Declaration of Helsinki as reflected in a priori approval by the Ethics Review Committee for Human Experimentation. Informed consent was obtained from each patient. The noncancerous liver tissues obtained from these patients were immediately frozen and stored at −80 °C until further use.

Taqman real-time RT-PCR was performed as described previously [24], using an ABI Prism 7700 Sequence Detector (Applied Biosystems, Foster City, CA). Primers and the TaqMan probe for *SOCS-1* were as follows:

Forward primer:5′-CTGGCCCCGGAGCAT-3′
Reverse primer:5′-GTTGTGTGCTACCATCCTACAGA-3′
Probe:5′-FAM-CCGGACGCTATGGCCCA-MGB-3′

Primers and probes for *SOCS-3*, β-*actin*, interferon regulatory factor (*IRF*)-1, c-*myc* and *bcl*-X_L genes were purchased from ABI by Assays-on-Demand system.

2.5. Methylation status

The methylation status of the *SOCS-1* gene was analyzed by methylation-specific PCR as described previously [20].

2.6. Western blotting and immunoprecipitation

Nuclear and cytoplasmic fractions were prepared from HepG2 cells, and Western blotting was performed as described previously [25]. Anti-STAT1 and anti-STAT3 polyclonal antibodies (Cell Signaling Technology, Inc., Beverly, MA), anti-phosphorylated STAT3 (Tyr705) polyclonal antibody (Cell Signaling Technology), anti-phosphorylated STAT3 monoclonal antibody (Upstate Biotechnology Inc., Lake Placid, NY), and anti-protein inhibitor of activated *STAT (PIAS)1*, *anti-PIAS3* and *anti-SOCS-1* antibodies (Santa Cruz Biotechnology, Inc., Santa Cruz, CA) were

used. Immunoprecipitation was done as described previously using antibodies followed by protein A-Sepharose [26].

2.7. Immunocytofluorescence

HepG2 cell lines with or without the core gene were grown overnight on chamber slides and treated with 10 ng/ml human IL-6 for 60 min. Cells were fixed with 4% paraformaldehyde plus methanol, and reacted with the anti-STAT3 antibody followed by incubation with a FITC-labeled secondary antibody.

2.8. Statistical analysis

The results are expressed as means±SD. The significance of the difference in means was determined by Mann–Whitney's *U*-test. $P<0.05$ was considered significant.

3. Results

3.1. HCV core protein suppresses SOCS-1 gene expression

To examine the impact of the core protein on *SOCS-1* gene expression, we analyzed mRNA expression levels by semi-quantitative RT-PCR in liver tissues from the HCV core gene transgenic and nontransgenic control mice. *SOCS-1* mRNA expression levels in mouse liver tissues of nontransgenic mice were increased in a dose-dependent manner of IL-6, but were only marginal in the liver tissues from the core gene transgenic mice even in those treated with the maximal dose of IL-6 (0.5 μg/g BW, $n=5$ each) (Fig. 1(A) and (C)). In contrast, the expression levels of *SOCS-3* mRNA in the core gene transgenic mice were comparable to or rather higher than those in nontransgenic mice, before and after stimulation with IL-6 (Fig. 1(A) and (E)) [27,28].

We then examined whether or not this observation in mice is reproducible in HepG2 cell lines that constitutively express the core protein. *SOCS-1* gene expression was suppressed in the core-expressing HepG2 cell lines Hep396, Hep397 and Hep39J, even after stimulation with IL-6, while control bulk HepG2 cells or a control Hepswx cell line expressed *SOCS-1* mRNA at high levels (Fig. 1(B) and (D)). In contrast, the levels of *SOCS-3* gene expression were similar among the core-expressing HepG2 cell lines and control HepG2 cells, and were augmented by stimulation with IL-6 (Fig. 1(B) and (F)). These observations indicate that the core protein selectively suppresses *SOCS-1* gene expression before the translational level. The SOCS-1 protein was not detectable by Western blotting either in the mouse liver or HepG2 cells using currently available anti-SOCS-1antibodies.

These results, obtained in HepG2 cell lines constitutively expressing the core protein, were then evaluated using a transient expression system. In this system, HepG2 cells were infected with baculovirus, expressing the core protein as described previously [29], and *SOCS-1* expression was determined by semiquantitative RT-PCR. The introduction

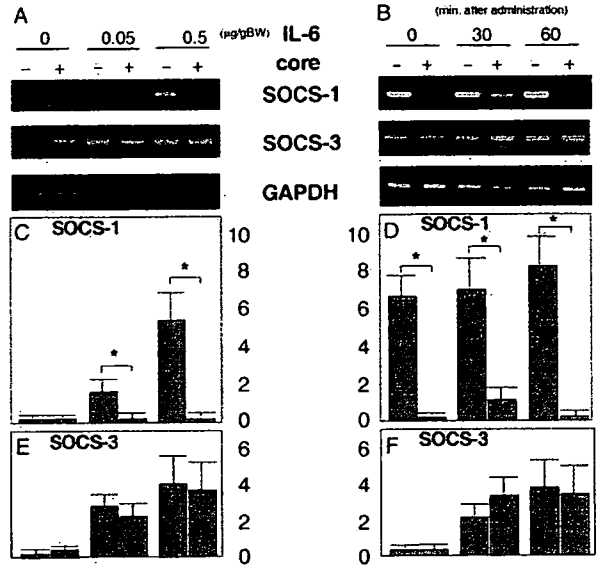

Fig. 1. Suppression of *SOCS-1* gene expression by hepatitis C virus core protein. (A) and (B) RNA from mouse liver tissues (A) or HepG2 cells (B) with or without the core protein was subjected to RT-PCR for the determination of *SOCS-1* and *SOCS-3* gene expression. Liver tissues were taken from mice one hour after inoculation of 0, 0.05 or 0.5 μg/g BW of IL-6. HepG2 cells (Hep396 and Hepswx) were treated with 10 ng/ml of IL-6 for 0, 30 or 60 min before RNA extraction. Bottom panels in (A) and (B) show the expression level of the housekeeping gene GAPDH as an internal control. (C) and (D) Represent means± SD. of five independent experiments on *SOCS-1* gene expression corresponding to the lanes in (A) and (B), respectively. *, $P<0.05$. (E) and (F) Represent means±SD. of five independent experiments on *SOCS-3* gene expression corresponding to the lanes in (A) and (B), respectively.

of the core protein selectively suppressed the expression level of *SOCS-1* mRNA even after stimulation with IL-6 (data not shown).

Modulation of expression by the core protein of STAT-target genes other than *SOCS*s was then examined by determining the mRNA levels in mouse liver tissues. Expression of *IRF-1* gene was suppressed in the presence of the core protein under the stimulation with IL-6, while that of c-*myc* was not affected (Fig. 2(A) and (B)). The expression of *bcl*-X_L gene was rather augmented by the core protein although the difference was not statistically significant (Fig. 2(C)).

The methylation status of *SOCS-1* gene was then explored in liver tissues from the core gene transgenic mice by a method described previously [20], to determine whether or not the *SOCS-1* gene expression may be suppressed by hypermethylation. No hypermethylation was observed in the *SOCS-1* gene of the core gene transgenic mice either at the 5′-noncoding region or the CpG island in the coding region (Fig. 3).

In the analysis of *SOCS-1* expression in noncancerous liver tissues from patients with HCV infection, the *SOCS-1* mRNA expression levels were 0.494±0.352 in HCV-positive patients ($n=9$) and 0.862±0.465 in the control subjects without HCV infection ($n=9$) (in arbitrary units,

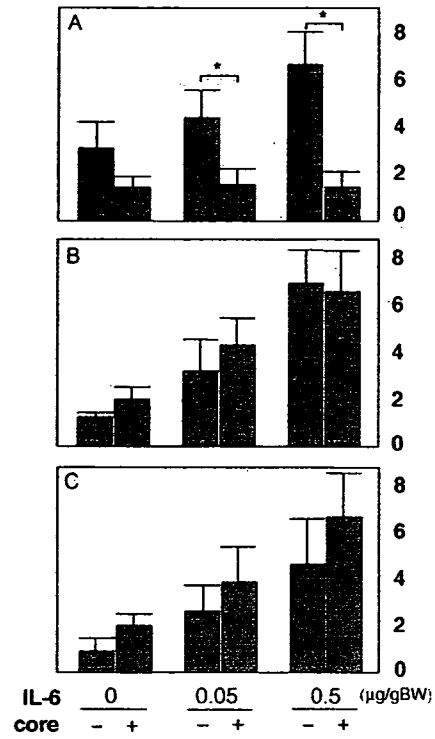

Fig. 2. Effect of hepatitis C virus core protein on the expression of STAT-target genes. RNA from mouse liver tissues with or without the core protein was subjected to RT-PCR for the determination of *IRF1* (A), c-*myc* (B) and *bcl*-X_L (C) gene expressions. Liver tissues were taken from mice one hour after inoculation of 0, 0.05 or 0.5 μg/g BW of IL-6. *, $P<0.05$.

$P=0.0345$). Thus, the SOCS-1 levels in the liver tissues of chronic hepatitis C patients were significantly lower than those of subjects without HCV infection.

3.2. The core protein did not suppress phosphorylation of STAT3 or STAT1

The activation of STAT3 enhances *SOCS-1* expression, thereby forming a negative feedback loop to the STAT3 status [17]. To determine whether or not STAT3 activation is involved in the *SOCS-1* gene suppression in this system, the tyrosine phosphorylation of STAT3 in the mouse liver was examined by Western blotting using an anti-phospho-STAT3 (tyrosine (Tyr)^{705}) antibody. At baseline, Tyr^{705} phosphorylation of STAT3 was low in both the core gene transgenic and nontransgenic mice. However, in response to stimulation with IL-6, the levels of Tyr^{705} phosphorylation of STAT3 was higher in the liver tissues from the core gene transgenic mice than that from nontransgenic mice. A representative result is shown in Fig. 4(A). Similarly, the levels of Tyr^{705} phosphorylation of STAT3 were higher in HepG2 cell lines expressing the core protein than those in control cells (Fig. 4(B)). These results observed in HepG2 cells constitutively expressing the core protein was also evaluated in a transient expression system using a recombinant baculovirus, as described above. The Tyr^{705} phosphorylation of STAT3 was enhanced in HepG2 cells infected with baculovirus expressing the core protein compared with mock-infected HepG2 cells (data not shown). The activation of STAT1 was also analyzed using HepG2 cell lines. As shown in Fig. 4(C), the levels of STAT1 phosphorylation was higher in HepG2 cells expressing the core protein than in control cells similar to the result on STAT3.

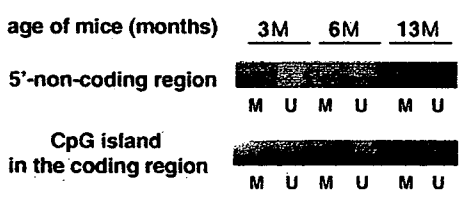

Fig. 3. Methylation status of *SOCS-1* gene in liver from hepatitis C virus core gene transgenic mice. DNA from the liver tissues of core gene transgenic mice at the age of 3 months (3M), 6 months (6M) or 13 months (13M) was subjected to methylation-specific PCR. Only PCR with unmethylation-specific primers yielded bands indicating that the *SOCS-1* gene was unmethylated in the liver tissues of core gene transgenic mice. M, methylation-specific primers; U, unmethylation-specific primers.

3.3. Subcellular localizations of STAT3 and STAT1

STAT activation by tyrosine phosphorylation results in the migration of STAT from the cytoplasm to the nucleus to bind to genomic DNA, modulating of cellular gene expression. We thereby evaluated the subcellular localization of STAT3 and STAT1 by preparing cytoplasmic and nuclear fractions from HepG2 cells followed by Western blotting. The amounts of STAT3 in the nuclei of core-expressing HepG2 cells were similar to or slightly larger

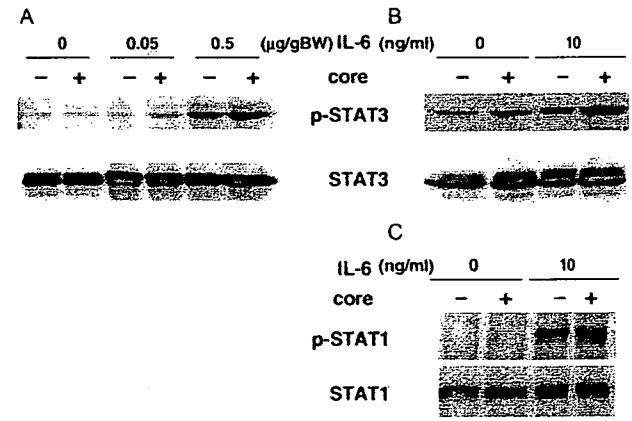

Fig. 4. Increase in the level of tyrosine phosphorylation of STAT3 and STAT1 by hepatitis C virus core protein. Whole cell lysates from mouse liver tissues (A) and HepG2 cells (B) and (C) were subjected to SDS-PAGE followed by Western blotting with anti-STAT3 and anti-*P*-STAT3 (A) and (B) or with anti-STAT1 and anti-*P*-STAT1 (C). Liver tissues were obtained from the mice treated as described in the Fig. 1 legends. HepG2 cells were treated with 10 ng/ml IL-6 or vehicle for 1 h. *P*-STAT3, phosphorylated STAT3; STAT3, total STAT3; p-STAT1, phosphorylated STAT1; STAT1, total STAT1. The experiments were repeated three times.

than those in control HepG2 cells in the presence or absence of IL-6 (Fig. 5(A)). This result was confirmed by an immunofluorescence study (Fig. 5(B)). A similar result was obtained in the analysis of STAT1 subcellular localization (Fig. 5(C)). These observations indicate that the HCV core protein does not inhibit the translocation of STAT3 or STAT1 to the nucleus, and the feedback mechanism is not the cause of *SOCS-1* gene suppression.

Because PIAS3 blocks the nuclear translocation of STAT3 or binding of STAT3 to genomic DNA [30], the expression of PIAS3 was examined by Western blotting. However, there was no significant difference in the levels of PIAS3 between core-expressing HepG2 cells and control HepG2 cells (data not shown). Co-immunoprecipitation analysis was also performed using HepG2 cell lines to know whether or not the core protein affects the association of PIAS1 with STAT1 or PIAS3 with STAT3. However, neither co-immunoprecipitation of STAT1 with anti-PIAS1 antibody nor that of STAT3 with anti-PIAS3 antibody was affected by the presence of the core protein (Fig. 6). We also examined the possibility of the interaction of the core protein with STAT3, which blocks the binding of STAT3 to the promoter of *SOCS-1* gene. For this purpose, a co-immunoprecipitation technique was utilized with whole-cell extracts of core-expressing HepG2 cells. However, no association was observed between these two proteins.

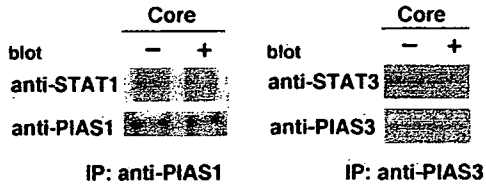

Fig. 6. Effect of the core protein on the interaction of STATs and PIASs. Cell lysates were immunoprecipitated with anti-PIAS1 or anti-PIAS3 antibody, and immunoblotted with anti-STAT1 or STAT3 antibody, respectively. There was no difference in the amounts of STAT1 or STAT3 that were co-immunoprecipitated with anti-PIAS antibodies.

4. Discussion

In the current study, we demonstrated that the core protein of HCV suppresses the expression of *SOCS-1* mRNA in the liver tissues of mice that develop HCC late in their life [4,7]. This observation was reproduced in cultured cells that expressed the core protein. This phenomenon may contribute to the modification of the IFN signaling systems

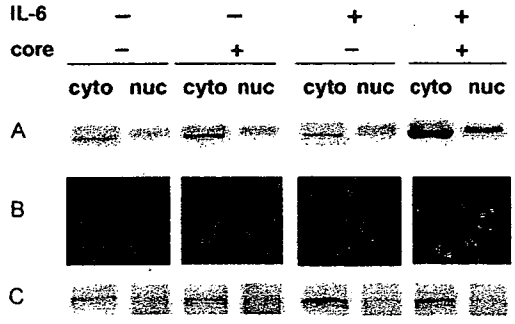

Fig. 5. Hepatitis C virus core protein did not affect subcellular localization of STAT3 or STAT1. Cytoplasmic and nuclear fractions from HepG2 cells with or without the core protein were subjected to Western blotting with the anti-STAT3 antibody (A) or anti-STAT1 antibody (C). HepG2 cells were fixed and an immunocytofluorescence study was performed using the anti-STAT3 antibody (B). Cells were processed before or 60 min after the treatment with 10 ng/ml of IL-6. cyto, cytoplasmic fraction; nuc, nuclear fraction [This figure appears in colour on the web].

in HCV infection, because SOCS-1 and SOCS-3 play central roles in the Jak/STAT pathway as negative feedback regulators [12–14]. In addition, since SOCS-1 also possesses a tumor suppressor activity [15–17], the down-regulation of *SOCS-1* may contribute to hepatocarcinogenesis in HCV infection. It has been reported that the silencing of the *SOCS-1* gene by hypermethylation is associated with the development of HCC [18–20]. Among patients with HCV infection, a major cause of chronic hepatitis worldwide, HCC develops at a very high incidence [1,2]. Hence, there may be an alternative mechanism of *SOCS-1* silencing to gene methylation in HCV infection. Our current data suggest a possibility of such a mechanism in that HCV per se acts as a negative regulator of SOCS-1, a tumor suppressor. The expression levels of *SOCS-1* mRNA in noncancerous liver tissues in chronic hepatitis C patients were also significantly lower than those in HCV-negative subjects, although the 'shut-off' of the *SOCS-1* gene observed in the experimental systems was not the case. This may be due to the presence of other factors influencing *SOCS-1* gene expression in vivo, including inflammation.

In the exploration of the mechanism underlying the down-regulation of *SOCS-1* expression, we first examined the methylation status of the *SOCS-1* gene in liver tissues from core gene transgenic mice by methylation-specific PCR. Neither the 5′-non-coding region nor the CpG island in the coding region of the *SOCS-1* gene [18–20] was hypermethylated, refuting methylation as a mechanism of SOCS-1 suppression.

We next determined whether or not STAT3, a transcription factor for the *SOCS-1* gene, is involved in the suppression of *SOCS-1* by the core protein: a decreased level or a disturbed phosphorylation of STAT3 may account for the suppression of *SOCS-1*. It was found, however, that STAT3 was rather activated by the core protein, consistent with a previous report [28]. The effect on STAT3 activation by the core protein is yet controversial [31]. Similarly, the activation and nuclear translocation of STAT1 was not disturbed by the presence of the core protein. The core protein differentially affected the expression of STAT-target genes such as *IRF1*, c-*myc* or *bcl*-X_L. The core protein suppressed *IRF1* expression in the mouse liver but did not those of c-*myc* and *bcl*-X_L genes. Regulation of *IRF1*

expression is STAT1-dependent in general, although STAT3 is also involved when stimulated by IL-6 [32]. c-*myc* and *bcl*-X_L inductions by IL-6 are chiefly mediated by STAT3 [33]. Thus, the modulation of expression by the core protein may occur in some other STAT-target genes, suggesting somewhere in Jak/STAT signaling pathway including STAT1 activation is impaired by the core protein. However, no defect was identified in the activation and nuclear translocation of STAT1 and STAT3 in the current study. Thus, although we could not define the precise role of the core protein in *SOCS-1* gene suppression, the direct effect of the core protein on the transcription of the gene is the most likely.

In summary, we found that the HCV core protein selectively suppresses *SOCS-1* gene expression in the liver tissues of animals and cultured cells. These findings may provide a basis for an alternative mechanism of the switch-off of SOCS-1 in the pathogenesis of HCV infection by modulating a tumor suppressor activity or responses to IFNs.

Acknowledgements

We thank Ms Y. Ogawa for her assistance in manuscript preparation. This work was supported by Grant-in-Aid for Scientific Research on Priority Area from the Ministry of Education, Science, Sports and Culture of Japan; Health Sciences Research Grants of The Ministry of Health, Welfare and Labor; The Program for Promotion of Fundamental Studies in Health Sciences of the Pharmaceuticals and Medical Devices Agency (PMDA); and grant from The Sankyo Foundation of Life Science.

References

[1] Saito I, Miyamura T, Ohbayashi A, Harada H, Katayama T, Kikuchi S, et al. Hepatitis C virus infection is associated with the development of hepatocellular carcinoma. Proc Natl Acad Sci USA 1990;87:6547–6549.

[2] Simonetti RG, Camma C, Fiorello F, Cottone M, Rapicetta M, Marino L, et al. Hepatitis C virus infection as a risk factor for hepatocellular carcinoma in patients with cirrhosis. Ann Intern Med 1992;116:97–102.

[3] Umeda T, Hino O. Molecular aspects of human hepatocarcinogenesis mediated by inflammation: from hypercarcinogenic state to normo- or hypocarcinogenic state. Oncology 2002;62:38–42.

[4] Koike K, Tsutsumi T, Fujie H, Shintani Y, Moriya K. Role of hepatitis viruses in hepatocarcinogenesis. Oncology 2002;62:29–37.

[5] Block TM, Mehta AS, Fimmel CJ, Jordan R. Molecular viral oncology of hepatocellular carcinoma. Oncogene 2003;22: 5093–5107.

[6] Colombo M. Hepatitis C virus and hepatocellular carcinoma. Semin Liver Dis 1999;19:263–269.

[7] Moriya K, Fujie H, Shintani Y, Yotsuyanagi H, Tsutsumi T, Ishibashi K, et al. The core protein of hepatitis C virus induces hepatocellular carcinoma in transgenic mice. Nat Med 1998;4: 1065–1067.

[8] Lerat H, Honda M, Beard MR, Loesch K, Sun J, Yang Y, et al. Steatosis and liver cancer in transgenic mice expressing the structural and nonstructural proteins of hepatitis C virus. Gastroenterology 2002;122:352–365.

[9] Moriya K, Nakagawa K, Santa T, Shintani Y, Fujie H, Miyoshi H, et al. Oxidative stress in the absence of inflammation in the liver of a mouse model for hepatitis C virus-associated hepatocellular carcinoma. Cancer Res 2001;61:4365–4370.

[10] Tsuchihara K, Hijikata M, Fukuda K, Kuroki T, Yamamoto N, Shimotohno K. Hepatitis C virus core protein regulates cell growth and signal transduction pathway transmitting growth stimuli. Virology 1999;258:100–107.

[11] Ray RB, Meyer K, Ray R. Hepatitis C virus core protein promotes immortalization of primary human hepatocytes. Virology 2000;271: 197–204.

[12] Starr R, Willson TA, Viney EM, Murray LJ, Rayner JR, Jenkins BJ, et al. A family of cytokine-inducible inhibitors of signaling. Nature 1997;387:917–921.

[13] Endo TA, Masuhara M, Yokochi M, Suzuki R, Sakamoto H, Mitsui K, et al. A new protein containing an SH2 domain that inhibits JAK kinases. Nature 1997;387:921–924.

[14] Naka T, Narazaki M, Hirate M, Matsumoto T, Minamoto S, Aono A, et al. Structure and function of a new STAT-induced STAT inhibitor. Nature 1997;387:924–929.

[15] Rottapel R, Ilangumaran S, Neale C, Rose JL, Ho JMY, Nguyen MHH, et al. The tumor suppressor activity of SOCS-1. Oncogene 2002;21:4351–4362.

[16] Ilangumaran S, Rottapel R. Regulation of cytokine receptor signaling by SOCS1. Immunol Rev 2003;192:196–211.

[17] Kishimoto T, Kikutani H. Knocking the SOCS off a tumor suppressor. Nat Genet 2001;28:4–5.

[18] Yoshikawa H, Matsubara K, Qian GS, Jackson P, Groopman JD, Manning JE, et al. SOCS-1, a negative regulator of the JAK/STAT pathway, is silenced by methylation in human hepatocellular carcinoma and shows growth-suppression activity. Nat Genet 2001; 28:29–35.

[19] Okochi O, Hibi K, Sakai M, Inoue S, Takeda S, Kaneko T, et al. Methylation-mediated silencing of SOCS-1 gene in hepatocellular carcinoma derived from cirrhosis. Clin Cancer Res 2003;9: 5295–5298.

[20] Miyoshi H, Fujie H, Moriya K, Shintani Y, Tsutsumi T, Makuuchi M, et al. Methylation status of suppressor of cytokine signaling-1 gene in hepatocellular carcinoma. J Gastroenterol 2004;39:563–569.

[21] Ruggieri A, Harada T, Matsuura Y, Miyamura T. Sensitization to Fas-mediated apoptosis by hepatitis C virus core protein. Virology 1997; 229:68–76.

[22] Aizaki H, Harada T, Otsuka M, Seki N, Matsuda M, Li YW, Kawakami H, et al. Expression profiling of liver cell lines expressing entire or parts of hepatitis C virus open reading frame. Hepatology 2002;36:1431–1438.

[23] Tsutsumi T, Suzuki T, Moriya K, Yotsuyanagi H, Shintani Y, Fujie H, et al. Alteration of intrahepatic cytokine expression and AP-1 activation in transgenic mice expressing hepatitis C virus core protein. Virology 2002;304:415–424.

[24] Tsutsumi T, Suzuki T, Moriya K, Shintani Y, Fujie H, Miyoshi H, et al. Hepatitis C virus core protein activates ERK and p38 MAPK in cooperation with ethanol in transgenic mice. Hepatology 2003;38: 820–828.

[25] Moriya K, Fujie H, Yotsuyanagi H, Shintani Y, Tsutsumi T, Matsuura Y, et al. Subcellular localization of hepatitis C virus structural proteins expressed in transgenic liver. Jpn J Med Sci Biol 1997;50:169–177.

[26] Tsutsumi T, Suzuki T, Shimoike T, Suzuki R, Moriya K, Shintani Y, et al. Interaction of hepatitis C virus core protein with retinoid X receptor-α modulates its transcriptional activity. Hepatology 2002;35: 937–946.

[27] Bode JG, Ludwig S, Ehrhardt C, Erhardt A, Albrecht U, Schaper F, et al. IFN-α antagonistic activity of HCV core protein involves induction of suppressor of cytokine signaling-3. FASEB J 2003;17:488–490.
[28] Yoshida T, Hanada T, Tokuhisa T, Kosai K, Sata M, Kohara M, et al. Activation of STAT3 by the hepatitis c virus core protein leads to cellular transformation. J Exp Med 2002;196:641–653.
[29] Shoji I, Aizaki H, Tani H, Ishii K, Chiba T, Saito I, et al. Efficient gene transfer into various mammalian cells, including non-hepatic cells, by baculovirus vectors. J Gen Virol 1997;78:2657–2664.
[30] Chung CD, Liao J, Liu B, Rao X, Jay P, Berta P, et al. Specific inhibition of Stat3 signal transduction by PIAS3. Science 1997;278:1803–1805.
[31] Hosui A, Ohkawa K, Ishida H, Sato A, Nakanishi F, Ueda K, et al. Hepatitis C virus core protein differently regulates the JAK-STAT signaling pathway under interleukin-6 and interferon-γ stimuli. J Biol Chem 2003;278:28562–28571.
[32] Kojima H, Nakajima K, Hirano T. IL-6-inducible complexes on an IL-6 response element of the junB promoter contain Stat3 and 36 kDa CRE-like site binding protein(s). Oncogene 1996;12: 547–555.
[33] Kiuchi N, Nakajima K, Ichiba M, Fukada T, Narimatsu M, Mizuno K, et al. STAT3 is required for the gp130-mediated full activation of the c-myc gene. J Exp Med 1999;189:63–73.

Antitumor NK activation induced by the Toll-like receptor 3-TICAM-1 (TRIF) pathway in myeloid dendritic cells

Takashi Akazawa*, Takashi Ebihara†, Manabu Okuno*‡, Yu Okuda*‡, Masashi Shingai†, Kunio Tsujimura§, Toshitada Takahashi§, Masahito Ikawa¶, Masaru Okabe¶, Norimitsu Inoue‖, Miki Okamoto-Tanaka**, Hiroyoshi Ishizaki**, Jun Miyoshi**, Misako Matsumoto*†, and Tsukasa Seya*†,††

Departments of *Immunology, ‖Molecular Genetics, and **Molecular Biology, Osaka Medical Center for Cancer, Nakamichi 1-3-2, Higashinari-ku, Osaka 537-8511, Japan; †Department of Microbiology and Immunology, Hokkaido University Graduate School of Medicine, Kita-15, Nishi-7, Kita-ku Sapporo 060-8638, Japan; ‡Department of Molecular Immunology, Nara Institute of Science and Technology, Ikoma, Nara 631-0101, Japan; §Division of Immunology, Aichi Cancer Center Research Institute, Nagoya, Aichi 464-8681, Japan; and ¶Genome Information Research Center, Osaka University, Suita, Osaka 565-0871, Japan

Edited by Tadatsugu Taniguchi, University of Tokyo, Tokyo, Japan, and approved November 4, 2006 (received for review July 17, 2006)

Myeloid dendritic cells (mDCs) recognize and respond to polyI:C, an analog of dsRNA, by endosomal Toll-like receptor (TLR) 3 and cytoplasmic receptors. Natural killer (NK) cells are activated *in vivo* by the administration of polyI:C to mice and *in vitro* are reciprocally activated by mDCs, although the molecular mechanisms are as yet undetermined. Here, we show that the TLR adaptor TICAM-1 (TRIF) participates in mDC-derived antitumor NK activation. In a syngeneic mouse tumor implant model (C57BL/6 vs. B16 melanoma with low H-2 expresser), i.p. administration of polyI:C led to the retardation of tumor growth, an effect relied on by NK activation. This NK-dependent tumor regression did not occur in TICAM-1$^{-/-}$ or IFNAR$^{-/-}$ mice, whereas a normal NK antitumor response was induced in PKR$^{-/-}$, MyD88$^{-/-}$, IFN-$\beta^{-/-}$, and wild-type mice. IFNAR was a prerequisite for the induction of IFN-α/β and TLR3. The lack of TICAM-1 did not affect IFN production but resulted in unresponsiveness to IL-12 production, mDC maturation, and polyI:C-mediated NK-antitumor activity. This NK activation required NK-mDC contact but not IL-12 function in *in vitro* transwell analysis. Implanted tumor growth in IFNAR$^{-/-}$ mice was retarded by adoptively transferring polyI:C-treated TICACM-1-positive mDCs but not TICAM-1$^{-/-}$ mDCs. Thus, TICAM-1 in mDCs critically facilitated mDC-NK contact and activation of antitumor NK, resulting in the regression of low MHC-expressing tumors.

antitumor immunity | type I interferon | syngenic tumor | implant model | gene-disrupted mice

Enhancing host immunity and increasing tumor antigenicity long have been goals of immunotherapy. Rosenberg *et al.* (1) summarized the results of 440 cancer patients who received a peptide vaccine. The overall objective response rate for all vaccine treatments was just 2.6% (1). Although their criteria for clinical objective response were strict, the results clearly reflect a limited effectiveness of the sole peptide vaccine therapy approach. Tumor cells often have diminished MHC class I (2), thereby circumventing the host immune surveillance system. They suggested that further technical exploration would be required, including additional manipulations of the vaccination procedure to establish effective tumor immunotherapy. Adjuvants are known to serve largely as ligands for Toll-like receptors (TLRs) (3, 4) and have the potential to compensate for the weakness of the peptide vaccine therapy. We have elucidated some of the roles of adjuvant in immunotherapy (5).

CTL and natural killer (NK) cells are two major cellular effectors against tumors. CTL mainly eliminate tumors with high levels of MHC class I proteins, whereas NK cells target tumors with low MHC levels. We have studied the profiles of effector induction in myeloid dendritic cells (mDCs) stimulated with adjuvants (5). In human and mouse, the bacillus Calmette–Guérin-cell-wall skeleton acts as a TLR2/4 agonist and induces mDC maturation followed by tumor-specific CTL in a syngeneic tumor implantation model if the tumors express MHC class I (5). Tumor regression and CTL induction largely relied on the MyD88 adapter-dependent pathway of TLR (5). Exogenously added tumor antigen (Ag) and adjuvant induce the mDCs cross-priming, which is required for MHC class I-mediated Ag presentation and CTL induction (6, 7). However, an MHC-negative population of the implant tumor survives to proliferate even after CTL induction. NK cells barely are activated in wild-type mice via the TLR2/4-MyD88 responses (5). Thus, MyD88-independent cellular responses are crucial in NK-mediated tumor cytotoxicity.

The TLR3 agonist polyI:C and TLR3 signaling in mDCs are able to regress tumors (6). TLR3 links TICAM-1 (or TRIF) in the cytoplasmic domain TIR (Toll-IL-1R homology domain) for signal transmission (8, 9). This adapter is unique in possessing two arrays of signals that activate two transcription factors, NF-κB and interferon (IFN) regulatory factor-3 (8–10). The latter is a strong inducer of type I IFN, particularly IFN-β (10–12). Recent reports suggest an important role for type I IFN in p53 induction (13) and cancer immunoediting (14). Type I IFN has been reported to be an inducer of various NK functions *in vitro* (15). Amplification of type I IFN production by IFNAR governs the expression of a number of IFN-inducible genes (16). These genes may be crucial for the functional modulation of mDCs.

mDCs and NK cells reciprocally activate one another during the immune response (15, 17). Several *in vitro* studies have shown that direct cell-cell contact as well as cytokines, including IFN-γ IL-12, and TNF-α, are involved in NK activation by mDCs (15, 17, 18). However, *in vivo* the molecular mechanism for reciprocal mDC maturation and NK activation has not been elucidated.

Here, we have investigated the mechanism whereby exogenously administered polyI:C induces tumor regression in gene-disrupted mice. We noticed that the retardation in the growth of MHC-negative tumors largely depended on the NK activity induced by polyI:C-stimulated mDCs. Using TICAM-1 (TRIF)$^{-/-}$ C57BL/6 mice [supporting information (SI) Fig. 7]

Author contributions: T.A., M.M., and T.S. designed research; T.A., T.E., M. Okuno, Y.O., and M.S. performed research; K.T., T.T., M.I., M. Okabe, M.O.-T., H.I., and J.M. contributed new reagents/analytic tools; N.I., M.M., and T.S. analyzed data; and T.S. wrote the paper.

The authors declare no conflict of interest.

This article is a PNAS direct submission.

††To whom correspondence should be addressed. E-mail: seya-tu@med.hokudai.ac.jp.

Abbreviations: KO, knockout; mDC, myeloid dendritic cell; NK, natural killer; TLR, Toll-like receptor.

This article contains supporting information online at www.pnas.org/cgi/content/full/0605978104/DC1.

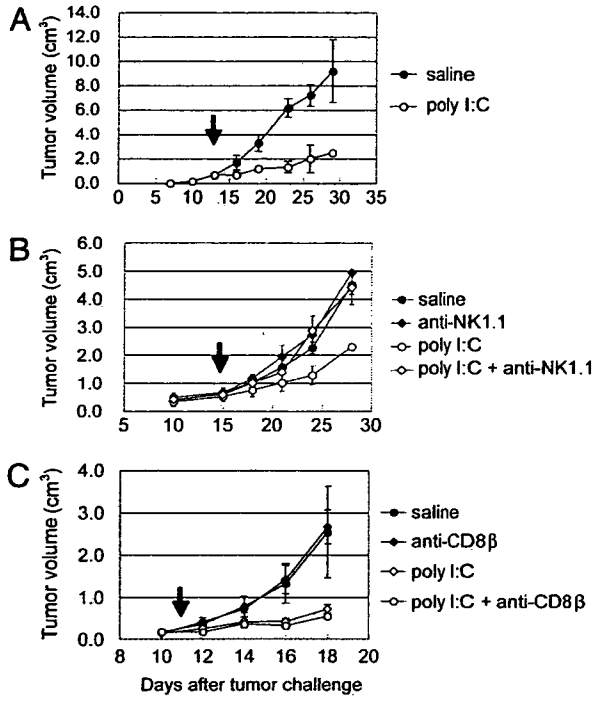

Fig. 1. PolyI:C induces NK-mediated MHC class I-negative tumor regression. (*A*) Establishment of tumor-implantation model for evaluation of polyI:C antitumor activity. PolyI:C (250 μg i.p. injected twice a week) caused antitumor effect on B16D8 cells (SI Fig. 8) implanted into C57BL/6 mice. Arrow indicates the start point of polyI:C treatment (tumor average size >0.8 cm³). (*B* and *C*) NK is an effector for poly(I:C)-mediated antitumor activity. Mice were challenged with B16D8 cells and i.p. injected with anti-NK1.1 (*B*) or anti-CD8β (*C*) ascites according to the schedule of polyI:C treatment (see *Materials and Methods*). Antibody and polyI:C treatment was repeated twice a week from day 10. One of the two similar experiments is shown.

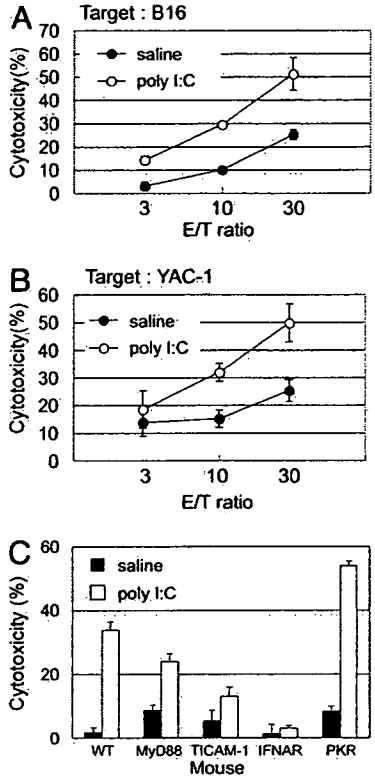

Fig. 2. Antitumor NK cells isolated from polyI:C-injected C57BL/6 mice. (*A*) *In vitro* B16 cytotoxicity by splenic NK cells of polyI:C-treated mice. C57BL/6 mice were administered with polyI:C (or control saline only) i.p. After 18 h, NK cells were isolated with MACS-negative selection beads and NK cytotoxicity against B16 cells was measured by ^{51}Cr release assay. (*B*) YAC-1 cytotoxicity of splenocytes was tested as in *A*. YAC-1 is known to be targets for NK. (*C*) NK activation depends on TICAM-1 and IFNAR. YAC-1 cytotoxicity of splenocytes from gene-disrupted mice stimulated with polyI:C. Indicated gene-disrupted mice were treated with polyI:C. After 18 h, splenocytes were prepared and their cytotoxicity against YAC-1 was measured by ^{51}Cr release assay. NK activation by polyI:C was impaired in splenocytes derived from IFNAR$^{-/-}$ or TICAM-1$^{-/-}$ mice. Effector-to-target cell ratio (E/T ratio) = 100. One of the three independent experiments is shown.

and a syngeneic tumor implant model, this NK activation was found to depend on direct contact of NK cells to mDCs, where NK activation is controlled by the TICAM-1 pathway of TLR in mDCs.

Results

Retardation of Tumor Growth by NK Cells in polyI:C-Treated Mice. PolyI:C is reported to induce type I IFN *in vivo* in mice and *in vitro* in mDCs (19, 20). Using a C57BL/6-B16 syngeneic tumor-implant model, we evaluated the antitumor activity of polyI:C, which was injected i.p. twice a week (Fig. 1*A*). Suppression of tumor growth, determined as reported in ref. 5, was observed in the group that received polyI:C compared with the saline-treated group. The retardation of tumor growth appeared to depend on polyI:C treatment but not on the level of MHC class I or a direct effect (such as apoptosis) on B16 cells (SI Figs. 8 and 9).

PolyI:C-mediated suppression of tumor growth was terminated when NK activity in mice was blocked by an injection of NK1.1 Ab (Fig. 1*B*) or asialo-GM1 Ab (data not shown). Thus, the polyI:C-mediated tumor suppression largely relies on the effector NK cells. Similar experiments by using another model (BALB/c vs. CT-26) and asialo-GM1 Ab confirmed the results obtained with the C57BL/6 vs. B16 model (data not shown).

Similar experiments by using the syngeneic mouse model were performed with CD8-eliminating Ab (Fig. 1*C*). Suppression of B16 tumor growth was not significantly changed by the treatment of mice with anti-CD8 Ab. CD8+ CTL-mediated tumor suppression is minimal, if any, in this model.

TICAM-1 and IFNAR Participate in NK Activation in Mice. We then assessed the tumor cytotoxicity of NK cells isolated from polyI:C-administered C57BL/6 mice. PolyI:C was administrated i.p. to mice, and the spleen cells were collected as a source of NK cells. To eliminate contaminating NKT cells, negative selection was performed to isolate NK cells by using MACS beads. NK cells efficiently expressed tumoricidal activity against the same lot of B16 melanoma cells (Fig. 2*A*). YAC-1 (an NK target) cells were killed in a fashion similar to B16 cells (Fig. 2*B*), supporting the view that NK is the effector. B16 and YAC-1 were used to measure the cytotoxicity of spleen cells collected from the indicated polyI:C-treated knockout (KO) mice (Fig. 2*C*). A significant decrease of cytotoxicity was observed in spleen cells prepared from IFNAR$^{-/-}$ or TICAM-1$^{-/-}$ mice. The polyI:C-mediated YAC-1 cytotoxicity was reduced only slightly in spleen cells of MyD88$^{-/-}$ mice. NK-mediated cytotoxicity increased in cells from PKR$^{-/-}$ mice. Similar results were obtained with B16 cells (data not shown).

To further confirm the results of Fig. 2*C*, B16 cells were implanted and tumor growth was followed *in vivo* in these KO mice. Retardation of B16 tumor growth by polyI:C was observed in MyD88$^{-/-}$, IFN-$\beta^{-/-}$, and PKR$^{-/-}$ mice at a level comparable to the control wild-type mice (Fig. 3). The antitumor activity of

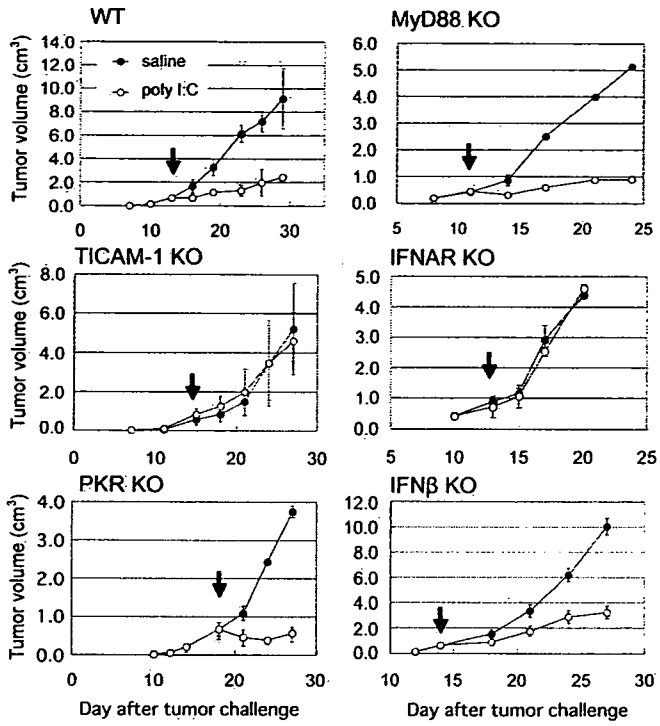

Fig. 3. Antitumor activity of PolyI:C depends on TICAM-1 and IFNAR *in vivo*. Antitumor effect of polyI:C on various KO mice were evaluated by using *in vivo* mouse tumor implant model. B16 tumor cells were inoculated on day 0. Arrow indicates the start point of polyI:C administration. Each point represents tumor size average ± SE ($n = 4$–6). The disrupted genes in mice are shown over the graphs.

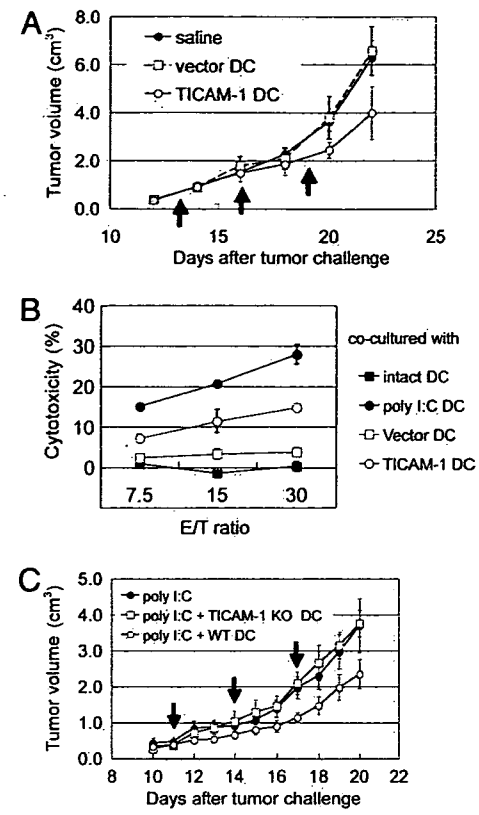

Fig. 4. TICAM-1 in mDCs is essential for antitumor activity of polyI:C. (*A*) Adoptive transfer of TICAM-1-transduced mDCs confers tumor growth suppression in mice. The lentiviral system was used for gene transfection into mDCs (SI Fig. 12). mDCs were prepared from bone marrow cells and transfected with TICAM-1 (TICAM-1 DC) or empty vector (vector DC). Wild-type mice were implanted with B16 cells on day 0. On day 12, 16, and 19, the mice with tumor burden were i.p. injected with TICAM-1-expressing mDCs (1×10^6 cells). Retardation of tumor growth was measured in the mice of control, with vector-containing mDCs or with TICAM-1-expressing mDCs. One of the three independent experiments is shown. (*B*) B16 killing by NK cells cocultured with mDCs. TICAM-1-expressing mDCs (TICAM-1 DC) and vector DC were prepared as in *A*. Poly I:C-stimulated mDCs (polyI:C DC) were prepared by incubation of mDCs with poly I:C for 4 h. The mDCs were cocultured with NK cells (DC:NK = 1:2) for 24 h. NK cytotoxicity against B16 was measured by ^{51}Cr release assay. (*C*) TICAM-1 in mDCs is required for polyI:C-mediated tumor regression. mDCs were prepared from wild-type and TICAM-1 KO mice. mDCs (3×10^6 cells) either from wild-type (WT DC) or TICAM-1 KO mice (TICAM-1 KO DC) and polyI:C (250 μg) were injected into the peritoneal cavity of IFNAR$^{-/-}$ mice, which had the tumor burden. Growth retardation of implanted tumor in response to polyI:C was measured in the mDC-injected mice. The arrows indicate the time points at which the mDCs were administered.

polyI:C diminished in TICAM-1$^{-/-}$ or IFNAR$^{-/-}$ mice (Fig. 3). Tumor regression by polyI:C was not affected by depletion of IFN-β, suggesting the participation of other IFNs (especially IFN-α) in the IFNAR-mediated antitumor response. These results infer that the antitumor activity by polyI:C is elicited through TICAM-1 and/or IFNAR in these mice. In the absence of IFNAR, no TLR3 was expressed by stimulation with polyI:C in mDCs (SI Fig. 10); therefore, the TLR3-TICAM-1 pathway does not function in IFNAR$^{-/-}$ mice. Taken together, the final effector for tumor killing is evidently NK cells activated in association with TLR3-TICAM-1 in this mouse tumor-implant model (Figs. 1 *B* and *C* and 3).

Mechanisms of NK Activation by polyI:C-Stimulated mDCs. The TICAM-1-dependent NK activation in polyI:C-treated mice was unexpected because polyI:C functions through multiple pattern-recognition receptors, i.e., PKR, RIG-I, and MDA5, in addition to TLR3 (21–23). All these receptors are induced by IFN-α/β in mDCs to recognize polyI:C *in vitro* (20). Although RIG-I and MDA5 were normally induced in TICAM-1$^{-/-}$ mDCs (SI Fig. 11), polyI:C-mediated NK activation was abolished in TICAM-1$^{-/-}$ mice (Fig. 3). We then aimed at clarifying the point that TICAM-1 in mDCs is responsible for the *in vivo* and *in vitro* antitumor NK activation by polyI:C.

TICAM-1 in mDCs participates in NK activation because adoptive transfer of mDCs with TICAM-1 overexpression (SI Fig. 12) also retarded tumor growth in wild-type mice (Fig. 4*A*). *In vitro* cytotoxic assay was performed with B16 cells and NK cells treated with TICAM-1-transduced mDCs (Fig. 4*B*). B16 cells were damaged by NK cells cocultured with polyI:C-treated mDCs, and to a lesser extent, with TICAM-1-transduced mDCs. Thus, mDCs expressing TLR3-TICAM-1 contribute to antitumor NK activation.

We next tested whether IFNAR in mDCs or other cells is important for mDC-mediated NK activation. IFNAR is distributed across mDCs and lymphocytes, including NK cells. The IFNAR$^{-/-}$ mice essentially failed to respond to polyI:C for tumor regression. When IFNAR-positive mDCs were transferred into IFNAR$^{-/-}$ mice, polyI:C-mediated antitumor NK activation was recovered in the IFNAR$^{-/-}$ mice (Fig. 4*C*). In contrast, no recovery of polyI:C-mediated tumor regression was observed by supplementing TICAM-1$^{-/-}$ mDCs into IFNAR$^{-/-}$ mice with the tumor burden (Fig. 4*C*). Thus, mDCs lead to tumoricidal NK activation in response to polyI:C *in vivo* and *in vitro*, where mDC TICAM-1 and IFNAR actively are involved.

The mechanism whereby TICAM-1 induces NK activation then was analyzed. Rae-1 proteins are up-regulated by TLR stimuli on murine macrophages and serve as ligands for NKG2D on NK cells (24). We checked the level of Rae-1 in mDCs. The Rae-1 level was not altered in response to polyI:C stimulation (SI Fig. 10). Next, we

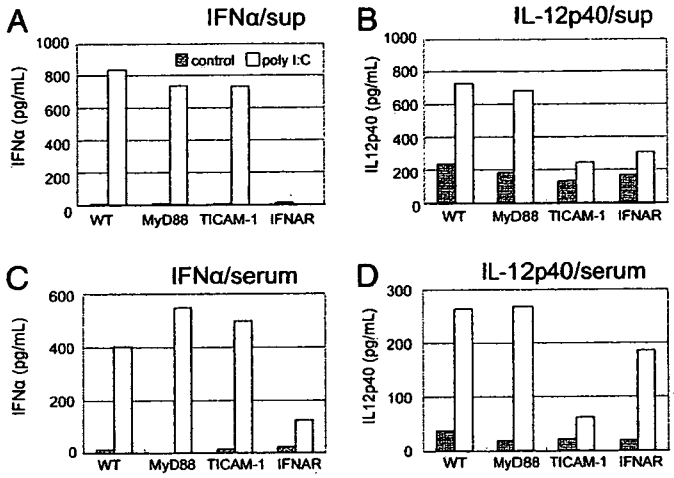

Fig. 5. Production of IFN-α and IL12p40 in response to poly I:C stimulation *in vivo* and *in vitro*. The concentrations of IFN-α and IL12p40 in cultured sup (*A* and *B*) of mDCs and in mouse serum (*C* and *D*) were determined by ELISA. mDCs were prepared from each KO mice and stimulated with 50 μg of polyI:C. After 24 h, culture supernatants were collected and the levels of cytokines (*A* and *B*) were measured. In other experiments, each indicated KO mouse was i.p. injected with polyI:C. After 16 h, blood was directly drawn from heart and clotted to collect serum (*C* and *D*). It is notable that IFNAR$^{-/-}$ mice failed to produce IFN-α *in vivo* and *in vitro*, but TICAM-1$^{-/-}$ mice retained IFN-producing capacity. Gray bars, controls with no stimulation; white bars, cells/mice stimulated with polyI:C. Figure represents one of four experiments.

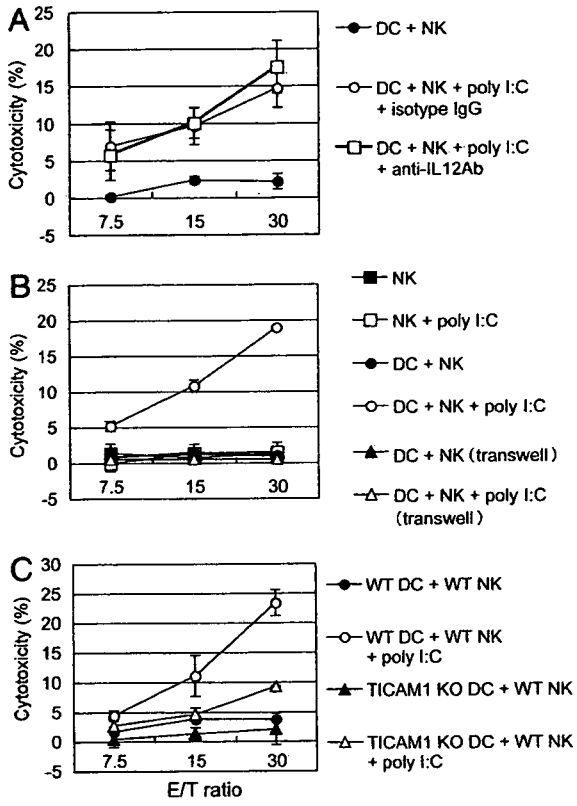

Fig. 6. mDCs activate NK cells via cell-cell contact, which depends on the TICAM-1 pathway. mDCs prepared from wild-type or TICAM-1 KO mice were incubated with poly I:C for 24 h, and NK cells were added to the culture at an mDC/NK ratio of 1:2. After 24 h, NK cells were incubated with B16 cells for 5 h at the indicated effector-to-target cell ratio (E/T ratio). Cytotoxicity of NK against B16 cells was examined by ^{51}Cr release assay. (*A* and *B*) NK cells were cocultured with mDCs in the presence of 5 μg/ml anti-IL12 antibody (*A*) or in the transwell system (*B*). (*C*) NK cells cocultured with mDCs derived from TICAM-1 KO mice.

measured the cytokine levels in the culture supernatant (sup) of polyI:C-stimulated mDCs prepared from gene-disrupted mice (Fig. 5 *A* and *B*). IFNAR$^{-/-}$ mDCs did not release IFN-α, whereas TICAM-1$^{-/-}$ mDCs and conventional (prepared from wild-type mice) and MyD88$^{-/-}$ mDCs released it by stimulation with polyI:C (Fig. 5*A*). There was only marginal up-regulation of IL-12 p40 (Fig. 5*B*) or mDC maturation (SI Fig. 13) by polyI:C in TICAM-1$^{-/-}$ and IFNAR$^{-/-}$ mDCs. However, mDCs are not merely a cell type producing IL-12 and type I IFN, and these cytokine profiles were somewhat discrepant in the serum of polyI:C-treated KO mice (Fig. 5 *C* and *D*). Furthermore, polyI:C-mediated tumor regression was not abolished by functional blockade of IL-12 in the B16 tumor implant model (SI Fig. 14), nor was the *in vitro* B16 tumor killing by NK cells cocultured with polyI:C-primed mDCs cancelled by the addition of IL-12-neutralizing Ab (Fig. 6*A*). The IL-12/IFN-α/β profiles in the serum are not consistent with the degrees of NK activation.

B16 killing due to NK cells activated by polyI:C-primed mDCs was impaired if spleen NK cells were cultured with polyI:C-primed mDCs in the transwell (Fig. 6*B*), suggesting that tumoricidal activity NK cells acquire via mDCs is attributable largely to cell-cell contact.

RIG-I and MDA5 as well as TLR3 and IFN-α/β are IFN-inducible genes that were up-regulated in the response of mDCs to polyI:C within 6 h (SI Fig. 11). The up-regulation was impaired in IFNAR$^{-/-}$ mice but not TICAM-1$^{-/-}$ mice (SI Fig. 11). We tested whether TICAM-1$^{-/-}$ mDCs stimulated with polyI:C still retain the activity to induce antitumor NK cells (Fig. 6*C*). Only weak antitumor NK activity was detected when the spleen NK cells were preincubated with TICAM-1$^{-/-}$ mDCs. Costimulator CD86 up-regulation in response to polyI:C also was impaired in the mDCs prepared from TICAM-1$^{-/-}$ as well as IFNAR$^{-/-}$ mice (SI Fig. 13). Thus, NK cell-binding molecules, rather than cytokines, are induced in mDCs through the TLR3-TICAM-1 pathway in response to exogenic dsRNA stimuli, which may explain the functional link between mDC TICAM-1 and NK activation.

Discussion

Here, we have demonstrated that TICAM-1 and IFNAR are involved in polyI:C-mediated maturation of mDCs and the generation of antitumor NK activity *in vivo* by using mouse models. Adoptive transfer of TICAM-1-positive mDCs but not TICAM-1-deficient mDCs exerted polyI:C-dependent suppression of tumor growth in IFNAR$^{-/-}$ mice (Fig. 4), suggesting that a unique TICAM-1-dependent response occurs in mDCs that elicits antitumor immunity. This effector is NK, a finding that is reinforced by the fact that the polyI:C-dependent tumor regression is abrogated largely by the administration of NK1.1 or asialoGM1 Ab. Thus, the NK-activating mDC subset is induced through the TICAM-1 pathway by the administration of polyI:C.

NK cells and mDCs are activated reciprocally via cytokines/IFNs and/or cell-to-cell contact (17). The molecular mechanism by which mDCs activate NK has not been clearly addressed. This study is demonstrates that the TICAM-1 pathway in mDCs serves to modulate mDCs to have NK-activating properties leading to the induction of tumoricidal NK activation.

Whereas TICAM-1 and IFNAR are not IFN-inducible, RIG-I, MDA5, TLR3, and IFN-α are IFN-inducible genes. They are rapidly up-regulated in response to polyI:C (SI Fig. 11). Thus, IFNAR is an indispensable factor for inducing TLR3 to complete the TLR3-TICAM-1 pathway and stimulate RIG-I/MDA5 to amplify IFN-α/β production. However, exogenously added IFN-α/β does not elicit NK-activating mDCs. Furthermore, adoptive transfer of TICAM-1-positive mDCs into IFNAR$^{-/-}$

mice with a tumor burden elicits an antitumor response. Thus, the type I IFN robustly produced by lymphocyte IFNAR barely participates in the elicitation of antitumor NK activity. Although MDA5 and RIG-I are normally induced by polyI:C in TICAM-$1^{-/-}$ mice with the ability to induce type I IFN (20, 23), mDCs in TICAM-$1^{-/-}$ mice have lost NK-activating activity in response to polyI:C. In fact, *in vitro* NK-mediated tumor-killing activity is minimally induced via coculture of NK cells with polyI:C-treated TICAM-$1^{-/-}$ mDCs (Fig. 6*C*). Cell-cell contact rather than IL-12 or IFN-α/β is closely associated with provoking NK-mediated tumor cytotoxicity (Fig. 6*B*). Hence, the NK-activating property depends only partly on cytokines or RIG-I/MDA5 but is rooted in the factors secondary to TICAM-1 in mDCs.

IFN-α/β and/or IL-12 p40 have been reported to be associated with NK activation *in vitro* (25). A primary role of pDCs in IFN-α/β (26) and NK activation (25) has been reported. However, this is not the case in *in vivo* NK-mediated tumor suppression. The most likely route for the activation of tumoricidal NK cells is in mDCs consisting of endosomal TLR3 and TICAM-1. The identification of TICAM-1-inducing NK-activating molecules in mDCs will foster an elucidation of the mechanism by which mDCs take on the NK-activating phenotype.

Moderately successful targeting of TLR3 by dsRNA in breast cancer has been reported with certain side effects (27). These investigations have suggested the TLR3 on tumor cells is a specific trigger of apoptosis signaling. Thus, the main focus in those studies was on polyI:C as an inducer of apoptosis in tumor cells (28). Other *in vitro* studies have suggested that the TLR3 pathway in mDCs is involved in cross-priming and CTL induction (6, 29). In this study, we show that the TICAM-1 pathway in mDCs induces mDC maturation that, in turn, directs NK activation. dsRNA acts on mDCs and tumor cells and in mDCs has multiple targets, resulting in the exerting of CTL induction and/or NK activation, both of which are pivotal in antitumor immunity.

Ultimately, polyI:C-mediated NK activation can be assigned to certain NK-activating ligands induced through the TLR3-TICAM-1 pathway in mDCs. Target recognition by NK is determined by the balance of NK-activating and -inhibitory receptors (30). These receptor ligands are variably expressed on mDCs (31) as well as tumor cells (32). Identification of the NK-activating molecules inducible on mDCs by dsRNA should lead to novel antitumor strategies against a variety of tumors.

Materials and Methods

Mice, Cells, and Reagents. TICAM-$1^{-/-}$ mice were backcrossed more than eight times to adapt the C57BL/6 background. PKR$^{-/-}$ (33), TLR3$^{-/-}$ (19), MyD88$^{-/-}$ (34), IFN-$\beta^{-/-}$ (35), and IFNAR$^{-/-}$ mice (36) were provided by T. Taniguchi (University of Tokyo, Tokyo, Japan) and S. Akira (Osaka University). All of the mice were maintained under specific pathogen-free conditions in the animal facility of the Osaka Medical Center and the Graduate School of Medicine Hokkaido University. They were backcrossed with C57BL/6 mice 8 to 10 times before use. Animal experiments were performed according to the guidelines set by the animal safety center, Japan.

B16D8 cell line was established in our laboratory as a subline of B16 melanoma (37). This subline was characterized by its low or virtually no metastatic properties when injected s.c. into syngeneic C57BL/6 mice (37). The mouse YAC-1 (BALB/c origin) cell line was provided by Sumitomo (Osaka, Japan), as described in ref. 32. These cell lines were cultured in RPMI medium 1640/10% FCS. Mouse NK cell was isolated with MACS Beads (Miltenyi Biotec, Auburn, CA). Bone marrow-derived mDCs were prepared as reported in ref. 38 with minor modifications.

Tumor Challenge and polyI:C Treatment. Mice were shaved at the flank and injected s.c. with 300 μl of 6×10^5 syngeneic B16D8 melanoma cells in PBS. After 1 week, tumor volumes were measured at regular intervals by using a caliper. Tumor volume was calculated by using the formula: Tumor volume (cm^3) = (long diameter) $\times$ (short diameter) $\times$ (thickness) $\times$ 0.4. PolyI:C was injected i.p. at a concentration of 250 μg per head. The treatments were started on day 10–14 (when average of tumor volume reached at 0.5–0.8 cm^3) and were repeated twice a week.

To deplete CD8+ T cells and NK cells *in vivo*, mice were i.p. injected with hybridoma ascites of anti-CD8β mAb and anti-NK1.1 mAb (39). All doses of antibodies and treatment regimens were determined in preliminary studies by using the same lots of antibodies used for the experiments. Treatment was confirmed to deplete completely the desired cell populations for the entire duration of the study.

TICAM-1 Gene-Transfected mDC Therapy. mDCs were transfected with mouse TICAM-1 cDNA by Lenti-viral transfection system (Invitrogen, Carlsbad, CA). The preparation and propagation of lentivirus were performed as follows (31). A sequence of hrGFP with the multicloning site with hrGFP was cloned from pIRES-hrGFP-1a vector (Stratagene, La Jolla, CA) and placed into the cloning site of pLenti6/V5-D-TOPO vector (Invitrogen) by TOPO-cloning system to add optimal restriction enzyme site to the 3′ terminal end of the target gene. This vector was named as pLenti-IRES-hrGFP. We used this empty vector as control. More than 50% of mDCs were GFP-positive after treatment with pLenti-IRES-hrGFP (data not shown).

Mouse TICAM-1 cDNA was cloned as described in ref. 4. In most experiments, a cDNA encoding the N-terminal region of TICAM-1 (1–550 aa) (40) was used instead of the full-length TICAM-1 cDNA, because the full-length TICAM-1 expression led to cell apoptosis within 8 h after transfection. The cDNAs were subcloned and sequenced for confirmation. The cDNAs were ligated into pLenti-IRES-hrGFP vector. The virus dose was determined so as to reach 50% GFP expression in mDCs 36 h after infection (31). Transfection efficiency was checked by using mDCs. Briefly, percent GFP-positive cells was estimated by flow cytometry or counting the cells under illumination of a fluorescence microscope as reported in ref. 41. Virus particles were prepared for transfection according to the manufacturer's protocol.

Assessment of NK Cytolytic Activity. Cytolytic activity of splenocytes and purified NK cells derived from polyI:C-treated mice was determined by ^{51}Cr-release assay. Mice were i.p. injected with 250 μg of polyI:C. After 16 h, mice were killed and splenocytes were isolated by using Lympholyte-M. NK cells were purified with MACS-negative selection beads. Target cells were labeled with ^{51}Cr for 3 h at 37°C, then washed and coincubated with effector cells at the indicated lymphocyte-to-target cell ratio in V-bottom 96-well plates in a total volume of 200 μl of RPMI medium 1640. Cytotoxicity was determined by measuring the ^{51}Cr radioactivity released in 100 μl of the supernatant harvested from the plate after 8 h of incubation at 37°C (32). The percentage of specific lysis was calculated by using the formula: %Specific lysis = [(experimental release − spontaneous release)/(total release − spontaneous release)] $\times$ 100.

Supporting Information. For additional details, see *SI Materials and Methods* and SI Table 1.

We thank Dr. K. Toyoshima (RIKEN, Yokohama, Japan) for organizing this project, the laboratory members for invaluable discussions, Drs. T. Taniguchi (University of Tokyo) and S. Akira (Osaka University) for providing gene-disrupted mice, and Dr. Boru (Pacific Edit) for reviewing this manuscript. This work was supported in part by CREST and Japan Science and Technology Corporation (JST), Grants-in-Aids from the Ministry of Education, Science, and Culture (Specified Project for Advanced Research) and the Hepatitis C Virus project in National Institutes of Health of Japan, and by the Naito Memorial Foundation, Uehara Memorial Foundation, Mitsubishi Foundation, and Takeda Foundation.

1. Rosenberg SA, Yang JC, Restifo NP (2004) *Nat Med* 10:909–915.
2. Seliger B, Maeurer MJ, Ferrone S (1997) *Immunol Today* 18:292–299.
3. Seya T, Akazawa T, Matsumoto M, Begum NA, Azuma I, Toyoshima K (2002) *Anticancer Res* 23:4369–4376.
4. Medzhitov R, Janeway CA, Jr (1997) *Cell* 91:295–298.
5. Akazawa T, Masuda H, Saeki Y, Matsumoto M, Takeda K, Akira S, Azuma I, Toyoshima K, Seya T (2004) *Cancer Res* 64:757–764.
6. Schulz O, Diebold SS, Chen M, Naslund TI, Nolte MA, Alexopoulou L, Azuma YT, Flavell RA, Liljestrom P, Reis e Sousa C (2005) *Nature* 433:887–892.
7. Datta SK, Redecke V, Prilliman KR, Takabayashi K, Corr M, Tallant T, DiDonato J, Dziarski R, Akira S, Schoenberger SP, Raz E (2003) *J Immunol* 170:4102–4110.
8. Oshiumi H, Matsumoto M, Funami K, Akazawa T, Seya T (2003) *Nat Immunol* 4:161–167.
9. Yamamoto M, Sato S, Hemmi H, Hoshino K, Kaisho T, Sanjo H, Takeuchi O, Sugiyama M, Okabe M, Takeda K, Akira S (2003) *Science* 301:640–643.
10. Fitzgerald KA, McWhirter SM, Faia KL, Rowe DC, Latz E, Golenbock DT, Coyle AJ, Liao SM, Maniatis T (2003) *Nat Immunol* 4:491–496.
11. Mori M, Yoneyama M, Ito T, Takahashi K, Inagaki F, Fujita T (2004) *J Biol Chem* 279:9698–9702.
12. tenOever BR, Servant MJ, Grandvaux N, Lin R, Hiscott J (2002) *J Virol* 76:3659–3669.
13. Takaoka A, Yanai H, Kondo S, Duncan G, Negishi H, Mizutani T, Kano S, Honda K, Ohba Y, Mak TW, Taniguchi T (2005) *Nature* 434:243–249.
14. Dunn GP, Bruce AT, Sheehan KC, Shankaran V, Uppaluri R, Bui JD, Diamond MS, Koebel CM, Arthur C, White JM, Schreiber RD (2005) *Nat Immunol* 6:722–729.
15. Hamerman JA, Ogasawara K, Lanier LL (2005) *Curr Opin Immunol* 17:29–35.
16. Taniguchi T, Takaoka A (2002) *Curr Opin Immunol* 14:111–116.
17. Fernandez NC, Lozier A, Flament C, Ricciardi-Castagnoli P, Bellet D, Suter M, Perricaudet M, Tursz T, Maraskovsky E, Zitvogel L (1999) *Nat Med* 5:405–411.
18. Gerosa F, Baldani-Guerra B, Nisii C, Marchesini V, Carra G, Trinchieri G (2002) *J Exp Med* 195:327–333.
19. Honda K, Sakaguchi S, Nakajima C, Watanabe A, Yanai H, Matsumoto M, Ohteki T, Kaisho T, Takaoka A, Akira S, *et al.* (2003) *Proc Natl Acad Sci USA* 100:10872–10877.
20. Kato H, Takeuchi O, Sato S, Yoneyama M, Yamamoto M, Matsui K, Uematsu S, Jung A, Kawai T, Ishii KJ, *et al.* (2006) *Nature* 441:101–105.
21. Yang YL, Reis LF, Pavlovic J, Aguzzi A, Schafer R, Kumar A, Williams BR, Aguet M, Weissmann C (1995) *EMBO J* 14:6095–6106.
22. Yoneyama M, Kikuchi M, Natsukawa T, Shinobu N, Imaizumi T, Miyagishi M, Taira K, Akira S, Fujita T (2004) *Nat Immunol* 5:730–737.
23. Gitlin L, Barchet W, Gilfillan S, Cella M, Beutler B, Flavell RA, Diamond MS, Colonna M (2006) *Proc Natl Acad Sci USA* 103:8459–8464.
24. Hamerman JA, Ogasawara K, Lanier LL (2004) *J Immunol* 172:2001–2005.
25. Degli-Esposti MA, Smyth MJ (2005) *Nat Rev Immunol* 5:112–124.
26. Honda K, Yanai H, Negishi, H, Asagiri M, Sato M, Mizutani T, Shimada N, Ohba Y, Takaoka A, Yoshida N, Taniguchi T (2005) *Nature* 434:772–777.
27. Khan AL, Richardson S, Drew J, Larsen F, Campbell M, Heys SD, Ah-See AK, Eremin O (1995) *Surgery* 118:531–538.
28. Salaun B, Coste I, Rissoan MC, Lebecque SJ, Renno T (2006) *J Immunol* 176:4894–4901.
29. Iwasaki A, Medzhitov R (2004) *Nat Immunol* 5:987–995.
30. Cerwenka A, Lanier LL (2001) *Nat Rev Immunol* 1:41–49.
31. Dull T, Zufferey R, Kelly M, Mandel RJ, Nguyen M, Trono D, Naldini L (1998) *J Virol* 72:8463–8471.
32. Masuda H, Saeki Y, Nomura M, Hirahashi T, Matsumoto M, Ui M, Lanier LL, Seya T (2002) *Biochem Biophys Res Commun* 290:140–145.
33. Mailliard RB, Son YI, Redlinger R, Coates PT, Giermasz A, Morel PA, Storkus WJ, Kalinski P (2003) *J Immunol* 171:2366–2373.
34. Adachi O, Kawai T, Takeda K, Matsumoto M, Tsutsui H, Sakagami M, Nakanishi K, Akira S (1998) *Immunity* 9:143–154.
35. Takaoka A, Mitani Y, Suemori H, Sato M, Yokochi T, Noguchi S, Tanaka N, Taniguchi T (2000) *Science* 288:2357–2360.
36. Muller U, Steinhoff U, Reis LF, Hemmi S, Pavlovic J, Zinkernagel RM, Aguet M (1994) *Science* 264:1918–1921.
37. Tanaka H, Mori Y, Ishii H, Akedo H (1988) *Cancer Res* 48:1456–1459.
38. Inaba K, Pack M, Inaba M, Sakuta H, Isdell F, Steinman RM (1997) *J Exp Med* 186:665–672.
39. Uno T, Takeda K, Kojima Y, Yoshizawa H, Akiba H, Mittler RS, Gejyo F, Okumura K, Yagita H, Smyth MJ (2006) *Nat Med* 12:693–698.
40. Oshiumi H, Sasai M, Shida K, Fujita T, Matsumoto M, Seya T (2003) *J Biol Chem* 278:49751–49762.
41. Shingai M, Inoue N, Okabe M, Akazawa T, Miyamoto Y, Ayata M, Honda K, Kurita-Taniguchi M, Matsumoto M, Ogura H, *et al.* (2005) *J Immunol* 175:3252–3261.

Differential Type I IFN-Inducing Abilities of Wild-Type versus Vaccine Strains of Measles Virus[1]

Masashi Shingai,[2]* Takashi Ebihara,* Nasim A. Begum,[3]† Atsushi Kato,‡ Toshiki Honma,‡ Kenji Matsumoto,‡ Hirohisa Saito,‡ Hisashi Ogura,§ Misako Matsumoto,*† and Tsukasa Seya[4]*†

Laboratory adapted and vaccine strains of measles virus (MV) induced type I IFN in infected cells. The wild-type strains in contrast induced it to a far lesser extent. We have investigated the mechanism for this differential type I IFN induction in monocyte-derived dendritic cells infected with representative MV strains. Laboratory adapted strains Nagahata and Edmonston infected monocyte-derived dendritic cells and activated IRF-3 followed by IFN-β production, while wild-type MS failed to activate IRF-3. The viral IRF-3 activation is induced within 2 h, an early response occurring before protein synthesis. Receptor usage of CD46 or CD150 and nucleocapsid (N) protein variations barely affected the strain-to-strain difference in IFN-inducing abilities. Strikingly, most of the IFN-inducing strains possessed defective interference (DI) RNAs of varying sizes. In addition, an artificially produced DI RNA consisting of stem (the leader and trailer of MV) and loop (the GFP sequence) exhibited potential IFN-inducing ability. In this case, however, cytoplasmic introduction was needed for DI RNA to induce type I IFN in target cells. By gene-silencing analysis, DI RNA activated the RIG-I/MDA5-mitochondria antiviral signaling pathway, but not the TLR3-TICAM-1 pathway. DI RNA-containing strains induced IFN-β mRNA within 2 h while the same recombinant strains with no DI RNA required >12 h postinfection to attain similar levels of IFN-β mRNA. Thus, the stem-loop structure, rather than full genome replication or specific internal sequences of the MV genome, is required for an early phase of type I IFN induction by MV in host cells. *The Journal of Immunology,* **2007, 179: 6123–6133.**

The type I IFNs represent a family of soluble cytokines with biological and antiviral activity (1, 2). In acute-phase viral infection, IFNs are secreted from affected cells via activation of IFN-inducing signal pathways. Recently, how virus induces type I IFNs is a focus for investigation and it was found that virus nucleotides trigger activation of the intracellular molecular cascades for the IFN production. In vertebrates, nucleic acid-sensing receptors recognize viral nucleotides to induce the production of type I IFNs. Endosomal TLRs, TLR3 (3, 4), TLR7 (5, 6), and TLR9 (7), cytoplasmic PKR (8), and retinoic acid-inducible gene I (RIG-I)[5]-like RNA-recognition receptors (9, 10), function as viral RNA sensors and individually induce type I IFNs through their pathways. These pathways involve activation of IRF-3 transcription factor, which is crucial for promoter activation of IFN-β (1). Type I IFNs act in either an autocrine or paracrine fashion by inducing the expression of hundreds of genes that together establish an antiviral state, which restricts the spread of virus around neighboring cells. In addition, type I IFNs enhance the function of NK cells (11, 12) and the differentiation of virus-specific CTL (13). Although the exact mechanism by which these effectors are induced in virus-infected hosts remains unknown, this innate response to viral patterns triggers a various array of antiviral immunity and eliminate virus-infected cells.

Many viruses have developed mechanisms to circumvent the host antiviral responses, thus potentially augmenting early spread of virus (14, 15). Viral strategies include inhibition of cytoplasmic RNA sensors RIG-I or melanoma differentiation-associated gene 5 (MDA5), blocking IFN regulatory factor-3 (IRF-3)-activating signals of the IFN system, and interfering with IFNR response by modulating the JAK-STAT-1 pathway (14, 15). Viral proteins are known to associate these IFN-inhibitory modes (15). Some virus species may harbor other inhibitory modes for IFN production. In contrast, there appears a strain-to-strain difference in virus-mediated IFN-α/IFN-β induction. Low IFN-inducing viruses can actively suppress the IFN production of the high IFN-inducing strains. These findings have barely been analyzed in conjunction with the various inhibitory modes of virus molecules and host receptors for IFN signaling.

*Department of Microbiology and Immunology, Graduate School of Medicine, Hokkaido University, Sapporo, Japan; †Department of Immunology, Osaka Medical Center for Cancer, Osaka, Japan; ‡Department of Allergy and Immunology, National Research Institute for Child Health and Development, Tokyo, Japan; and §Department of Virology, Osaka City University, Osaka, Japan

Received for publication February 12, 2007. Accepted for publication July 27, 2007.

The costs of publication of this article were defrayed in part by the payment of page charges. This article must therefore be hereby marked *advertisement* in accordance with 18 U.S.C. Section 1734 solely to indicate this fact.

[1] This work was supported in part by CREST and Innovation, Japan Science and Technology Corporation, and by Grants-in-Aid from the Ministry of Education, Science, and Culture (Specified Project for Advanced Research), and the Hepatitis C Virus Project in National Institutes of Health of Japan, and by the Takeda Foundation, the Uehara Memorial Foundation, the Mitsubishi Foundation, the Akiyama Foundation, and the NorthTec Foundation.

[2] Current address: National Institute of Allergy and Infectious Diseases, National Institutes of Health, Bethesda, MD 20892.

[3] Current address: Department of Molecular Biology, Graduate School of Medicine, Kyoto University, Kyoto, Japan.

[4] Address correspondence and reprint requests to Dr. Tsukasa Seya, Department of Microbiology and Immunology, Graduate School of Medicine, Hokkaido University, Kita-ku, Sapporo 060-8638 Japan. E-mail address: seya-tu@pop.med.hokudai.ac.jp

[5] Abbreviations used in this paper: RIG-I, retinoic acid-inducible gene; MDA5, melanoma differentiation-associated gene 5; IRF, IFN regulatory factor; MV, measles virus; p.i., postinfection; mDC, myeloid DC; DI, defective interference; CHO, Chinese hamster ovary; pAb, polyclonal Ab; MOI, multiplicity of infection; siRNA, small interference RNA; TBK1, TANK-binding kinase 1; IKKε, IκB kinase-related kinase ε; MAVS, mitochondria antiviral signaling; ISRE, IFN-stimulated response element; Q-PCR, quantitative PCR; NAP1, NAK-associated protein 1; CIAP, calf intestine alkaline phosphatase; SeV, Sendai virus; VISA, virus-induced signaling adaptor.

In measles virus (MV), wild-type strains barely induce production of significant quantities of IFN-α/IFN-β (16). In contrast, measles vaccine strains, including the attenuated Edmonston (ED) strain, are efficient IFN inducers that cause part of the attenuation of virulence. The wild-type MV strains actually suppress IFN production induced by coinfected MV ED infection (16). Furthermore, 10 passages of the wild-type MVs on Vero cells are sufficient to transform their phenotype from an IFN suppressor to an IFN inducer (16). These earlier studies stressed the total output of IFN production, measuring the IFN-α/IFN-β content >24 h postinfection (p.i.; late phase), thus the event involving replication and translation of viral genome RNA. Yet, the possible participation of viral V and C proteins in the IFN production has not been sufficiently considered under the contemporary knowledge (15). The molecular basis of strain-specific IFN-inducing ability, therefore, remains largely undetermined.

We have compared the IFN-α/IFN-β induction and sensitivity of the laboratory passaged attenuated MV strains with those of recent wild-type viruses isolated and passaged on human PBMC, the B95a marmoset B cell line, or early passage lots of Vero cells. We found that the majority of vaccine and laboratory adapted MV strains rapidly induced the IFN-β mRNA within 12 h p.i. (early phase) independent of viral protein translation. A further finding was that the robust production of IFN-β in human myeloid dendritic cells (mDCs) and epithelial cells paralleled the elevating of the level of virus-specific defective interfering RNA (DI RNA). The DI RNAs are subviral replicons originating from the viral genome and are associated with many RNA viruses (17). Wild-type MV isolates induced significantly lower production of IFN in mDCs and they contained undetectable levels of DI RNA. Thus, we speculate that DI RNA in MV isolates is a crucial determinant for high IFN induction in MV laboratory adapted and vaccine strains.

Materials and Methods

Cell culture and reagents

The human lung epithelial cell line (A549), A549/CD150, African green monkey kidney cell line (Vero), Vero/CD150, HEK293, and 293-3-46 cells (kindly provided by M. A. Billeter, University of Zurich, Zurich, Switzerland) were maintained in DMEM supplemented with 10% heat-inactivated FCS (JRH Biosciences) and antibiotics. Chinese hamster ovary (CHO), CHO/CD46, and CHO/CD150 (18) were cultured in Eagle's MEM with 5% heat-inactivated FCS. B95a cells were grown in RPMI 1640 supplemented with 5% heat-inactivated FCS and antibiotics. Cells were kept in 5% CO_2 at 37°C incubator. Vero/CD150 was established according to the method by Ono et al. (19). For establishing CD150-expressing A549 and Vero sublines, $pCNX_2$-huCD150, an expression plasmid for human CD150 bearing a neomycin-resistance gene was introduced into A549 cells using Lipofectamine 2000 (Invitrogen Life Technologies) according to the manufacturer's recommendation. Two days after transfection, the neomycin analog G418 (Sigma-Aldrich) was added to the medium at the final concentration of 1 or 2 mg/ml for A549 or Vero cells. During the selection, G418-containing medium was changed once every 4 days. G418-resistant, stably transfected clones were propagated for the study of surface expression of CD150 by FACS. Poly I:C was purchased from Amersham. Mouse mAbs against human CD150 (IPO-3) was purchased from eBioscience and mAbs against human CD46 (M75 and M177) were produced in our laboratory (20). Rabbit polyclonal Ab (pAb) against human CD150 or human CD46 was produced in our laboratory (21). HRP-conjugated goat anti-rabbit Igs were obtained from American Qualex Manufacturers.

Virus preparation and titration

Nagahata (NV) and Edmonston (ED) strains were obtained from the Research Institute for Microbial Diseases (Osaka University, Osaka, Japan) and University of Washington (Seattle, WA), respectively. Ichinose (IC)-B and IC-V were provided from Drs. F. Kobune (National Institutes of Health, Tokyo, Japan) and K. Takeuchi (Tsukuba University, Tsukuba, Japan) (22). Wild-type MV strains were from Osaka University, Osaka City University, and Osaka Prefectural Research Institute. Masusako (MS) and other strains of MV were propagated in our laboratory (21, 23, 24). Vaccine strains of MV were purchased from Takeda, Tanabe, and Banyuu (Osaka, Japan). ED, NV, IC-V, MS, Yokota, CAM, AIK-C, Schwarz, and Tanabe strains were maintained in Vero cells in our laboratory. MS and Yokota strains are early passage lots (<10 passages). IC-B, Na-PBMC, Suz-PBMC, MOE, HY, Moka, and Kishida strains were maintained in B95a cells as reported (22). Virus titer was determined as PFUs on Vero/CD150 and the multiplicity of the infection (MOI) of each experiment was calculated based on this titer (19). For Ab blocking of measles virus entry receptors, cells were pretreated with pAb (35 μg/ml) against human CD46 or human CD150, or mAb (5 μg/ml) against human CD150 or human CD46 for 1 h before the virus infection (25).

Preparation of human monocyte-derived immature dendritic cells and macrophages

Human PBMC were isolated from buffy coat of normal healthy donors by methylcellulose sedimentation followed by standard density gradient centrifugation with Ficoll-Hypaque (Amersham Bioscience) (26). For human immature mDC and macrophage preparations, $CD14^+$ monocytes were obtained from human PBMC by using MACS system (Miltenyi Biotec) with anti-human CD14 mAb-conjugated microbeads. For mDCs, $CD14^+$ monocytes were kept in RPMI 1640 containing 10% FCS, 500 IU/ml human GM-CSF, 100 IU/ml human IL-4 (PeproTech) and antibiotics for 6 days. For macrophages, $CD14^+$ monocytes were kept in RPMI 1640 containing 10% FCS, 500 IU/ml human GM-CSF, and antibiotics for 9 days. Morphological changes were examined by phase contrast microscopy (Olympus IX-70).

Determination of human IFN-β level

For the estimation of secreted IFN-β, culture medium were centrifuged to remove cell debris and the supernatants were stored at −80°C until the assay. The level of secreted human IFN-β in the culture medium was determined according to the manufacturer's protocol using ELISA kit (Fujirebio).

FACS cytometric analysis of cell surface Ags

Methods for FACS analyses were described previously (26). Briefly, cells were suspended in PBS containing 0.1% sodium azide and 1% BSA (FACS buffer) and incubated for 30 min at 4°C with anti-CD46, CD150, or isotype control, washed, followed by FITC-labeled anti-mouse IgG $F(ab')_2$. Cells were washed and fluorescence intensity was measured by FACS.

Expression profile analysis with GeneChip

All microarray experiments and their data were analyzed according to Minimum Information About a Microarray Experiment (MIAME) guidelines. Total RNA from mDCs was extracted by the RNeasy kit (Qiagen) according to the manufacturer's instructions. Total RNA (10 μg) from each sample was used to prepare cRNA. Gene expression was analyzed with GeneChip Human Genome U133A probe array (Affymetrix), which contains ~22,000 gene probe sets. Data analysis was performed with Affymetrix microarray suite software version 5 (MAS 5.0; Affymetrix) and GeneSpring software version 6.1 (Silicon Genetics). The default settings of MAS 5.0 were used to calculate scaled gene expression values for each sample.

Native PAGE, SDS-PAGE, and Western blotting

Whole cell extracts were prepared in 20 mM HEPES containing 25% (v/v) glycerol, 0.42 M NaCl, 1.5 mM $MgCl_2$, 0.2 mM EDTA, 0.5 mM PMSF, 0.5 mM DTT, 30 mM NaF, and 1 mM Na_3VO_4. Protein concentration of the lysate was measured by Bio-Rad protein assay kit. For detection of phosphorylated IRF-3, whole cell extracts (60 μg) were subjected to SDS-PAGE in a 7.5% polyacrylamide gel. Proteins were electrophoretically transferred to Immobilon-P (Millipore) and probed with 1/500 diluted anti-IRF-3 pAb (FL-425; Santa Cruz Biotechnology). Dimer formation of IRF-3 was observed by separating the cell extracts (20 μg) on 7.5% polyacrylamide gel native PAGE (Dai-ichi Pure Chemicals), transferred to membrane, and probed with anti-IRF-3 pAb (1/100 diluted; IBL), washed with PBS containing 0.5% Tween 20 three times and incubated with HRP-conjugated goat anti-rabbit Ig pAb for 1 h at 37°C. Following second incubation, the membranes were washed three times with PBS-Tween 20 and proteins were detected with an ECL chemiluminescence kit (Amersham Biosciences) (26).

RT-PCR and quantitative PCR (Q-PCR)

To remove the viruses attached on cell surface, cells were treated with trypsin, neutralized with serum containing medium, and washed three

Table I. *Cellular responses to various strains of MV*

Strains	IFN-β Production[a]	Syncytium[b]					
	DCs	DCs	Mϕ	CHO	CHO/CD46	CHO/CD150	Passage
Laboratory adapted strains							
ED	+	++	+	−	+++	+++	Vero
NV	++	+	+	−	++	++	Vero
IC-V	+	+	+	−	+	++	Vero
Wild-type strains							
MS	−	++	−	−	−	+++	Vero**
Yokota	−	++	−	−	−	+	Vero**
IC-B	−	++	−	−	−	+	B95a
Na-PBMC	−	++	−	−	−	+	B95a
Suz-PBMC	−	++	−	−	−	+	B95a
MOE	−	++	−	−	−	++	B95a
HY	−	++	−	−	−	++	B95a
Moka	−	++	−	−	−	++	B95a
Kishida	−	++	−	−	−	+	B95a
Vaccine strains							
CAM	+	+	+*	−	+	++	Vero
AIK-C	+	+	+*	−	+	++	Vero
Schwarz	+	+	+*	−	+	++	Vero
Tanabe	++	++	+*	−	+	++	Vero

[a] ++, >10 IU/ml; +, <10 IU/ml.
[b] +++, >60% CPE; ++, 30–60% CPE; +*, aggregated (atypical CPE); **, virus replicates in cells without syncytium formation; −, not detected.

times with ice-cold PBS. Total RNA was extracted with RNeasy mini kit (Qiagen), 2 μg of total RNA was incubated at 70°C for 5 min, kept on ice for 2 min, and reverse transcription was performed with Moloney murine leukemia virus-reverse transcriptase (Promega) at 37°C for 90 min followed by PCR or Q-PCR. For PCR, ex-*Taq*DNA polymerase (Takara) was used. Sequences of the primers used for RT-PCR were reported earlier (27). Reaction for Q-PCR was performed with iQ SYBER Green Supermix and amplified PCR products were measured by iCycler iQ real-time PCR analyzing system (Bio-Rad). Primers for PCR were designed using Primer Express software (PerkinElmer/Applied Biosystems). The following primers were used for Q-PCR: human β-actin forward, 5′-CCTGGCACCCA GCACAAT-3′; reverse, 5′-GCCGATCCACACGGAGTACT-3′; human IFN-β forward, 5′-CAACTTGCTTGGATTCCTACAAAG-3′; reverse, 5′-TATTCAAGCCTCCCATTCAATTG-3′; MV-H-forward 5′-CCCTTATC AACGGATGATCC-3′; reverse-5′-GTGATCAATGGCCCGAATCC-3′. Normalized value for each mRNA expression was calculated as relative quantity of mRNA divided by the relative quantity of human β-actin.

RNA interference

The method for gene-silencing using small interference RNA (siRNA) oligonucleotides was described previously (28). The method for transient gene-silencing using siRNA oligonucleotides was described previously (29). The sequences of the siRNA for TICAM-1 (29), TANK-binding kinase 1 (TBK1), IκB kinase-related kinase ε (IKKε) (30), RIG-I, MDA5, and mitochondria antiviral signaling (MAVS) (IPS-1/Cardif/VISA) (31) were reported previously. The method for establishing stable gene-silenced HeLa cells was reported in a preceding report (28). Knockdown status was analyzed by RT-PCR.

Reverse genetics to produce recombinant MV

MV323 (wild-type Ichinose strain) and MV2A (ED strain) were recovered from p^+MV323 and p^+MV2A, respectively, as previously described (27, 32). Briefly, 293-3-46 cells were transfected with p^+MV323 and p^+MV2A, plus L gene-expressing plasmid. Two days later, B95a cells were overlaid. Recovered viruses were amplified with Vero or Vero/CD150 cells.

p(−) MV minigenome replicon GFP and in vitro transcription of the RNA replicon

The vector p(−)MV minireplicon GFP was constructed for transcribing the MV minireplicon GFP RNA(−) as a MV short genome. MV minireplicon GFP RNA contains the leader sequence, noncoding region of the N gene, GFP gene, noncoding region of the L gene, and the trailer sequence. The cDNA of MV minireplicon GFP was inserted into pT7 MV vector (containing T7 promoter, T7 terminator, genomic hepatitis δ virus ribozyme) which was constructed by modifying p^+MV323 (provided Dr. K. Takeuchi, Tsukuba University) (32). MV minireplicon GFP RNA^- was transcribed from p^-MV minireplicon GFP RNA^+ using MEGAscript T7 kit (Ambion) in vitro. Calf intestine alkaline phosphatase (CIAP; Takara) treatment of the transcribed RNA was performed according to the manufacturer's protocol.

Plasmid transfection and luciferase assay

A luciferase reporter gene plasmid, pISRE-Luc (firefly luciferase, experimental reporter), was purchased from Stratagene, pRL-TK vector (*Renilla* luciferase for internal control) was obtained from Promega. All transfections were conducted on HEK293 cells growing in 24-well plates. Usually, 100 ng of pISRE-Luc and 3 ng of pRL-TK vector were introduced into cells according to the manufacturer's procedure (Qiagen). At 24 h posttransfection, synthetic MV minireplicon RNA or poly I:C was introduced into cells by Lipofectamine 2000 (Invitrogen Life Technologies). Six hours later, cells were harvested with trypsin, washed with PBS, and treated with 20 μl of passive lysis buffer (Promega) and the assay was performed using dual luciferase reporter assay system (26). Fold induction against the control medium is indicated.

RT-PCR amplification of cDNA from 5′ copy-back DI RNAs

We modified the RT-PCR amplification protocol of Calain (33), where the copy-back DI RNAs were amplified using two sets of MV primers (for 5′ copy-back DIs, JM396; 5′-TATAAGCTTACCAGACAAAGCT GGGAATAGAAACTTCG-3′/JM403;5′-CGAAGATATTCTGGTGTA AGTCTAGTA-3′, and for standard genome, JM396/JM402; 5′-TTTA TCCAGAATCTCAARTCCGG-3′) (34, 35). Viral RNA from the culture supernatant was extracted with QIAamp Viral RNA Mini kit (Qiagen). Total RNA from viral-infected cells was extracted with the RNeasy mini kit (Qiagen). Two micrograms of total RNA was incubated at 70°C for 5 min, kept on ice for 2 min, and reverse transcription was performed with Moloney murine leukemia virus-reverse transcriptase (Promega) at 37°C for 90 min followed by PCR. The PCR-amplified products were cloned into pCR blunt vector (Invitrogen Life Technologies) and sequencing was performed using the BigDye Terminator version 3.1 Cycle Sequencing kit (Applied Biosystem).

Results

MV attenuated strains induce IFN-β in mDC infection

Type I IFN-inducing activity of various MV strains was tested using mDCs by ELISA (Table I). Laboratory adapted strains ED, NV, and IC-V, and vaccine strains CAM, AIK-C, Schwarz, and Tanabe, all produced IFN-β in infected mDCs. These stains were propagated through Vero cells. CHO cells expressing either CD46

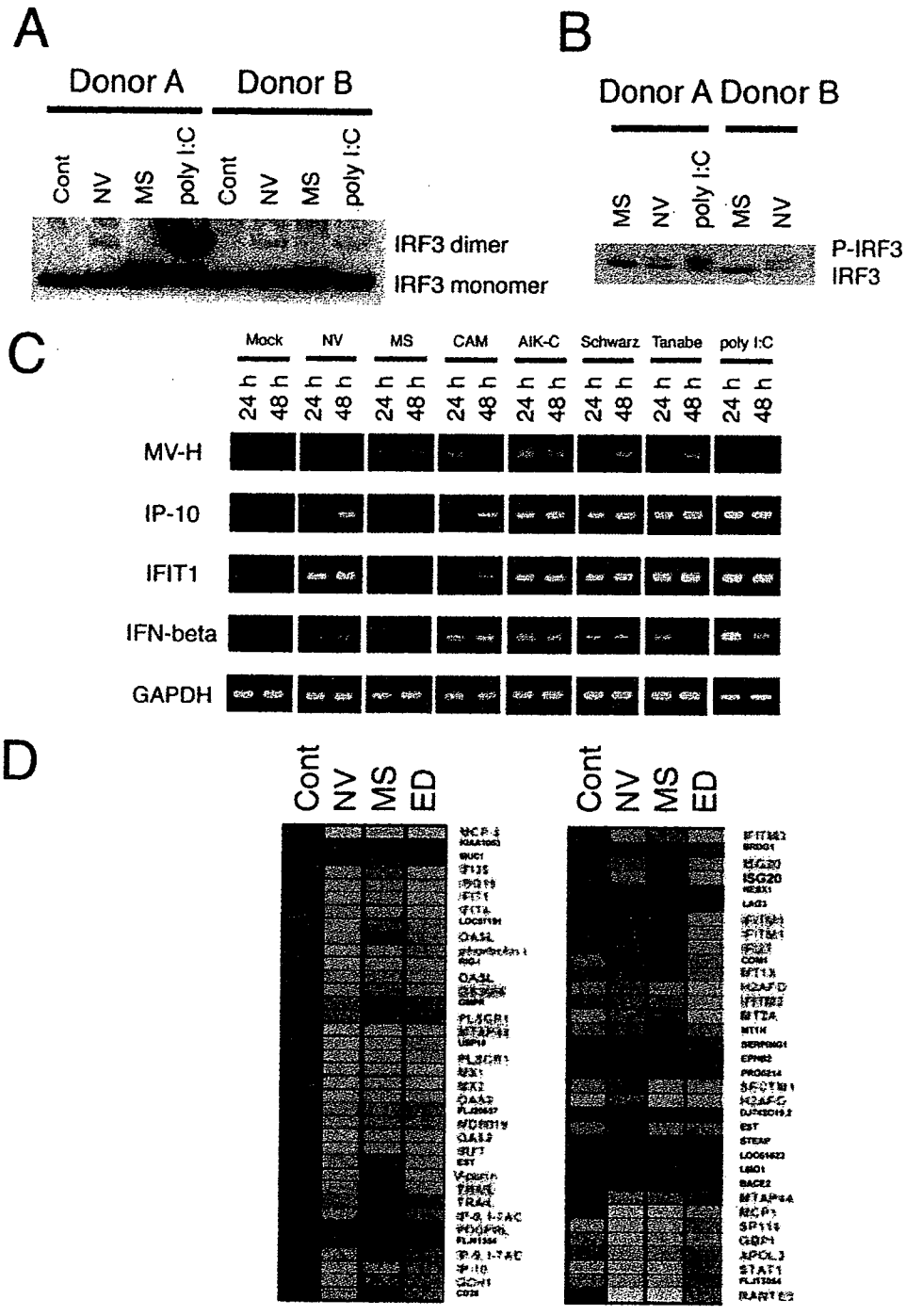

FIGURE 1. Laboratory adapted and vaccine strains highly induce type I IFN and IFN-inducible genes in monocyte-derived mDCs. Monocyte-derived mDCs were stimulated with medium alone (cont), poly I:C (10 μg/ml for 1 h), or MV strains (MOI = 1 typically for 8 h). At timed intervals, cells were lysed for IRF-3 analysis. CD46-adapted strain (NV or ED), CD46 nonadapted strain (MS), or vaccine strains (CAM, AIK-C, Schwarz, or Tanabe). *A*, Native gel analysis for IRF-3 dimerization; or *B*, SDS-PAGE for IRF-3 phosphorylation. *C*, At indicated intervals, MV-H, IP-10, IFIT1, IFN-β, and GAPDH mRNAs were detected using RT-PCR. *D*, Three major clusters of MV-regulated genes in mDCs infected with various MV strains. mDCs were infected with the indicated MV strains at MOI = 1. 8 h later, RNAs were extracted from the mDCs and analyzed by GeneChip. Data were analyzed by applying a hierarchical-tree algorithm to the normalized intensity. Induced genes are indicated by shades of red; repressed genes are indicated by shades of blue. Gene symbols are shown in the *right column*.

or CD150 formed syncytia when infected with these strains (Table I). In contrast, wild-type isolates largely established in Osaka were mostly passaged with B95a cells and barely produced IFN-β. Only CHO cells expressing CD150 formed syncytia by wild-type MV infection. Because the results on the receptor usage of these strains are consistent with ability of type I IFN induction, MV adaptation to the CD46 receptor might have linked the high IFN-inducing phenotype.

Defective IRF-3 activation in low IFN inducers of wild-type strains

Activation of IRF-3 was tested with human mDCs using representative laboratory adapted (NV, ED) and a Vero-adapted wild-type (MS) strain. NV and ED but not wild-type strain MS induced dimerization (Fig. 1*A*) and phosphorylation (Fig. 1*B*) of IRF-3. The results were confirmed with other laboratory adapted, vaccine, and wild-type strains (data not shown). Thus, strain-specific IRF-3 activation determines IFN-β induction in mDCs. NV and vaccine strains induced IFN-inducible genes, *IP-10*, *IFIT1*, and *IFN-β*, but the wild-type-strain including MS did not (Fig. 1*C*). An example of our comprehensive approaches regarding type I IFN-inducible genes are shown by microarrays using mRNAs from immature mDCs infected with representative strains (Fig. 1*D*). NV and ED strains, but not the MS strain, up-regulated IFN-inducible genes, supporting their high vs low IFN-β-inducing properties.

What factor is responsible for high IFN-β-inducing properties in MV?

The findings in Fig. 1 allowed us to surmise that NV and ED contain a factor that is responsible for higher induction of IFN-β

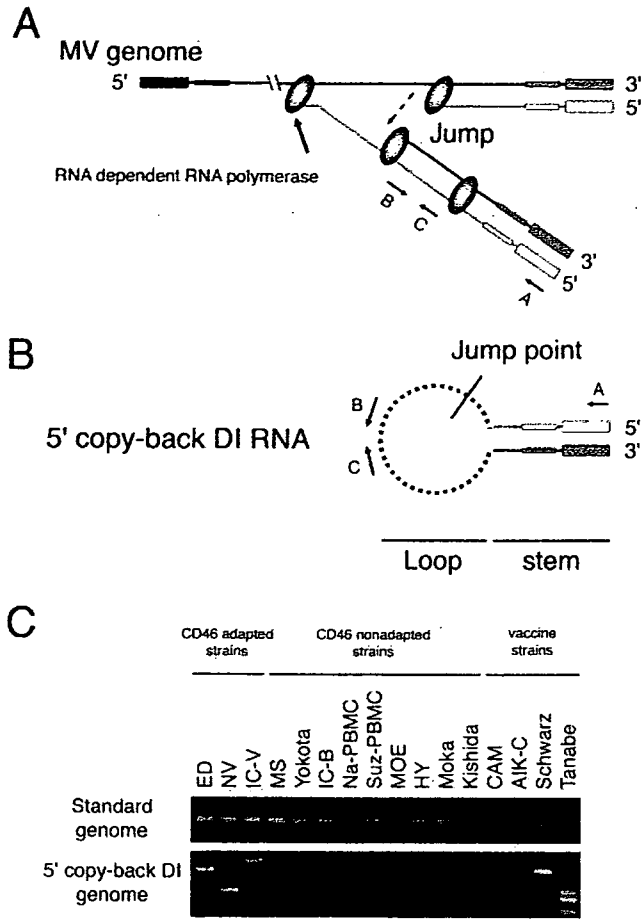

FIGURE 2. Laboratory adapted and vaccine strains contain 5′ copy-back DI RNA. *A*, Model for the origin of 5′ copy-back DI RNA. Two RNA polymerase complexes synthesized a negative-strand RNA from the positive-strand RNA template. The polymerase complex switches the template to a negative-strand RNA synthesized by a front RNA complex. *B*, The product perfectly matches with a part of the terminal and RNA duplex (stem). *C*, RT-PCR amplification of 5′ copy-back DI RNA from various strains of MV culture supernatants. RT-PCR was performed using standard genome-specific primers (primer A, JM396; and primer B, JM402, in the *upper panel*) or DI-specific primers (primer A, JM396; and C, JM403, in the *lower panel*).

and MS and other wild-type strains lack it. Then, the question is what factor participates in high IFN-β induction in MV laboratory adapted strains. NV and ED, but not MS, use CD46 as an entry receptor (18, 21). Both stimulation and mAb-blocking studies on the receptor CD46 suggested no direct participation of CD46 in IFN-β induction (M. Taniguchi and T. Seya, unpublished data). A previous report suggested the involvement of nucleocapsid (N) protein of MV in IFN induction (36, 37). Transfectants with N protein, however, did not induce IFN promoter activation (M. Shingai and T. Seya, unpublished data). N protein-expressing cells further transfected with MV RNA elevated IFN promoter activation compared with mock transfection with RNA alone (data not shown). Thus, these previous findings did not explain the differential induction of IFN-β in wild-type vs vaccine strains upon infected cells. Because the IFN-inducing ability of NV was dominant in cells coinfected with MS in an early phase, IFN-inducing rather than IFN-inhibitory factors (38) govern the IFN-inducing phenotype of MV in the early phase.

Our repetitive trials suggested that 5′ copy-back DI RNA has the ability to induce IFN-β. 5′ copy-back DI RNA was present in

Table II. *Properties of DI RNAs of MV strains*

Strains	DI Genome Size (nt)	Stem Size (nt)	Loop (nt)
ED	1152	142	868
NV	726	121	474
ICV	1385	120	1145
Schwarz	1098	177	744
Tanabe[a]	642	103	436
	618	98	422
	474	98	278

[a] At least three patterns were found in 12 clones.

most of the laboratory adapted and vaccine strains (Fig. 2*A*). By using the method of Calain and others (33–35), a unique primer set enabled us to detect 5′ copy-back DI RNA by RT-PCR (Fig. 2, *A* and *B*). Standard genome-specific primers are primer A (JM396) and B (JM402). DI RNA-specific primers are: primer A (JM396) and C (JM403). The standard genome RNAs were detected in the culture supernatants from all MV strains using RT-PCR amplified with primers A and B (Fig. 2*C*, *upper panel*). In contrast, the 5′ copy-back DI RNAs were detected in the culture supernatants of the laboratory adapted strains (NV, ED, and IC-V) and vaccine strains (Schwarz and Tanabe) using RT-PCR amplified with primers A and C (Fig. 2*C*, *lower panel*). The 5′ copy-back DI RNAs were not detected by this method in any wild-type strain or in CAM and AIK-C vaccine strains (Fig. 2*C*, *lower panel*). Amplified fragment sizes of the 5′ copy-back DI RNAs were variable depending on the strains cells were infected with. In Tanabe strains, multiple fragments were detected. These fragments were cloned

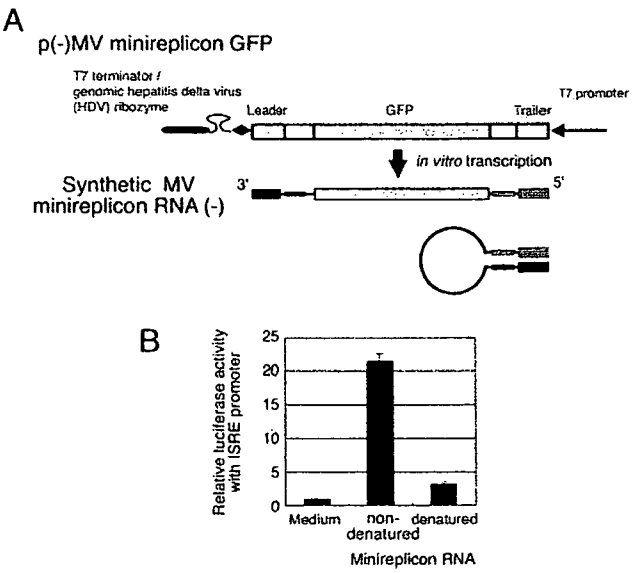

FIGURE 3. Viral minireplicon RNA induces IFN signaling. *A*, Schematic representation of vector p(−)MV minireplicon GFP and transcribed synthetic MV minireplicon GFP RNA⁻ (linear and stem loop forms). MV minireplicon GFP RNA(−) was transcribed using T7 in vitro transcription. Black boxes and gray boxes were highly complementary to a sequence element, which is present in 3′ and 5′ regions of the MV genome, suggesting that the synthetic MV minireplicon consists of stem and loop. *B*, Synthetic minireplicon RNA activates the ISRE promoter. HEK293 cells were transfected with pISRE-Luc and phRL-TK. Twenty-four hours later, cells were transfected with in vitro-transcribed MV minireplicon RNA, or heat-treated denatured MV minireplicon RNA. Six hours later, the cells were lysed and luciferase reporter assay was performed. The experiments were performed at least three times and a representative one is shown.

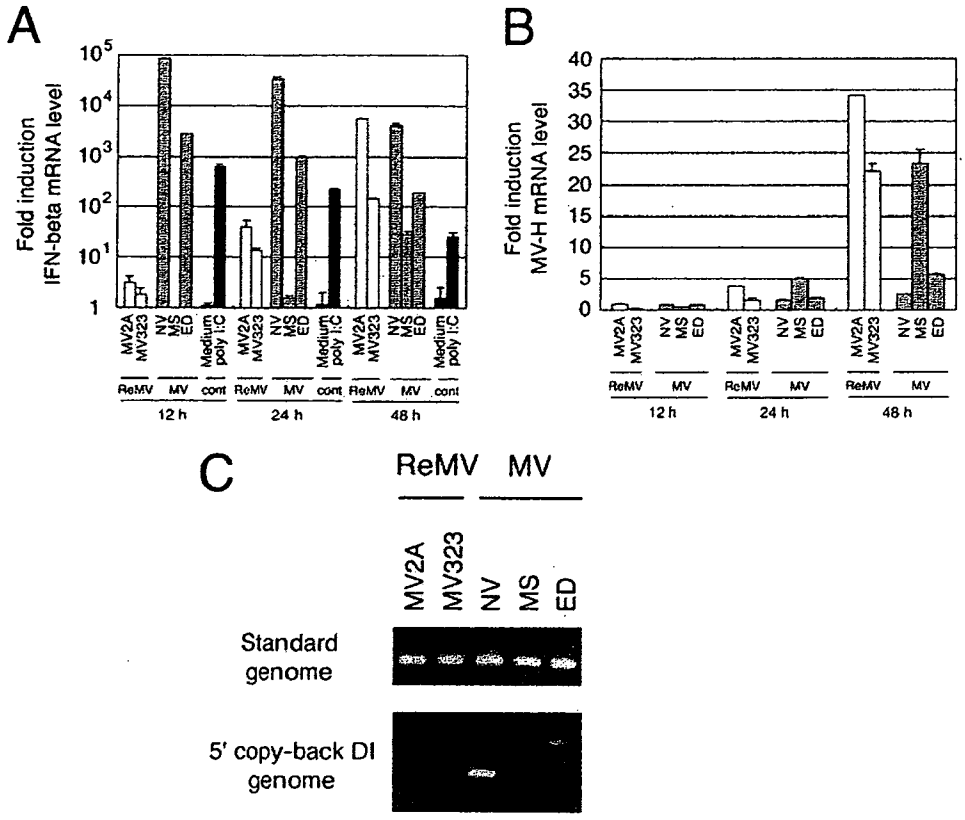

FIGURE 4. MV-containing DI RNA induces robust IFN-β in mDCs in an early phase. IFN-β induction and MV replication profiles in monocyte-derived mDCs. Monocyte-derived mDCs were infected with MV2A (rMV ED strain), MV323 (rMV IC-B strain), NV (laboratory adapted strain with DI RNA), MS (wild-type strain without DI RNA), or ED (laboratory adapted strain with DI RNA) at MOI = 0.1, or treated with medium or poly I:C (20 μg/ml). *A*, Twelve, 24, or 48 h after infection, the mRNA levels of human IFN-β in mDCs infected with each strain were measured by Q-PCR. The values were normalized to that of β-actin mRNA. Fold induction against medium at 12 h is shown. *B*, MV-H mRNA level was also measured by Q-PCR. The value for MV-H mRNA expression was normalized to that of β-actin mRNA. Relative fold induction against infection of each strain at 0 h is shown. Experiments were performed at least three times and representative results are shown. *C*, RT-PCR amplification of 5′ copy-back DI RNA from culture supernatants of rMVs (ReMVs; MV2A and MV323) or MVs (NV, MS, and ED). RT-PCR was performed as described in Fig. 2*C* using standard genome-specific primers (primers A and B, *upper panel*) or DI-specific primers (primers A and C, *lower panel*).

into the plasmid vector and sequenced. Their sizes and predicted structures are shown in Table II and Fig. 2*B*, where the sites of the primers are indicated for detection of DI RNA. Their predicted structures consisted of the stem and loop of various sizes in these DI RNAs (Fig. 2*B*, Table II).

The stem-loop RNA duplex induces IFN-stimulated response element (ISRE) promoter activation

We next examined whether the stem-loop structure of MV is crucial for type I IFN induction. The GFP sequence was inserted into the leader and trailer of MV (Fig. 3*A*). This synthetic RNA (named MV minireplicon RNA) has highly complementary sequence elements in 3′ and 5′ regions (black and gray boxes), which are needed for replication, transcription, and encapsidation. The synthetic MV minireplicon RNA forms the stem-loop containing RNA duplex by these complementary sequences (Fig. 3*A*). IFN-β-inducing activity of MV minireplicon RNA was examined by reporter assay in HEK293 cells. MV minireplicon RNA was either simply added to the cells or transfected by lipofection. When intact MV minireplicon RNA was transfected, luciferase activity with the ISRE promoter showed ~20-fold against that of medium control (Fig. 3*B*). Detectable levels of the ISRE promoter activation were seen only 6 h after the RNA administration (data not shown). Transfection of denatured MV minireplicon RNA resulted in the loss of IFN-inducing function (Fig. 3*B*). Thus, the stem-loop structure rather than the MV-specific RNA sequence may be essential for type I IFN elevated by MV DI RNA.

Measles virus ED strain with 5′ copy-back DI RNA highly induce IFN-β

Because 5′ copy-back DI RNAs forming the stem-loop structures with double helix induce IFN-β, we examined whether type I IFN induction by MV strains correlated with the amplitude of accompanied DI RNA. mDCs were infected with ED strain with DI RNA and rED strain (MV2A) without DI RNA at MOI = 0.1. The mRNA levels of IFN-β and MV-H in mDCs were determined by Q-PCR 12, 24, and 48 h p.i. (Fig. 4*A*). IFN-inducing activity of ED (with DI RNA) was high in an early phase (<12 h) of infection while that of MV2A was low. The IFN-β mRNA levels of cells infected with rMV2A (ED), MV323 (IC), and wild-type MS strain, all lacking DI RNAs, were low at 12 h p.i. and then increased in a time-dependent manner (Fig. 4*A*). Viral growth was monitored with the MV-H mRNA level. MV strains without DI RNAs efficiently replicated in mDCs in comparison with those with DI RNAs (Fig. 4*B*). Presence of DI RNAs in the lots of these MV strains was confirmed using RT-PCR (Fig. 4*C*). Similar results were obtained with A549/CD150 cells (data not shown). Thus, the induction of IFN-β is closely associated with coexisting DI RNAs in an early phase of MV infection.

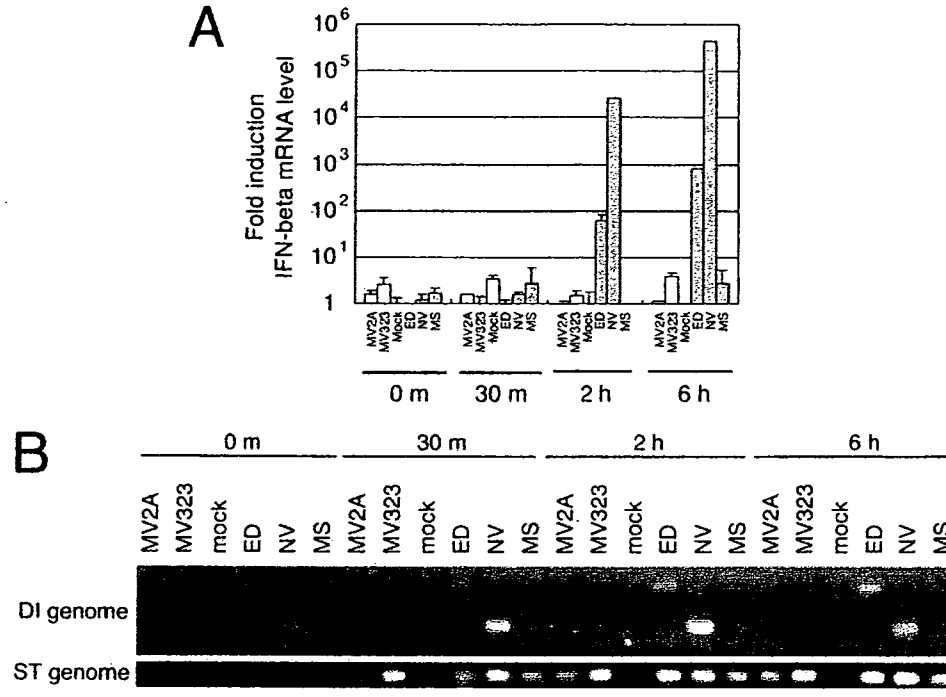

FIGURE 5. MV strain-specific IFN-β mRNA induction in infected cells. *A*, A549/CD150 cells without TLR3 were infected with mock, MV2A (rMV ED strain), MV323 (rMV IC-B strain), NV (laboratory adapted strain with DI RNA), MS (wild-type strain without DI RNA), or ED (laboratory adapted strain with DI RNA) at MOI = 0.1. At timed intervals, RNA samples were recovered and mRNAs of IFN-β and β-actin were measured by Q-PCR. The value for IFN-β mRNA expression was normalized to that of β-actin mRNA. Fold induction against control medium is shown. *B*, RT-PCR for DI RNA and the standard genome of MV was performed as in Fig. 2*C* using genome-specific primers (primers A and B, *upper panel*) or DI-specific primers (primers A and C, *lower panel*). Experiments were performed at least three times and representative results are shown.

In other experiments using A549/CD150 cells, parallelism between the levels of IFN-β mRNA (Fig. 5*A*) and the amplitude of DI RNA (Fig. 5*B*) was analyzed. DI RNA was detected over 30 min, then increased in a time-dependent manner (Fig. 5*B*). Thus, the initial source of DI RNA should be in the virion. Viral DI RNA was increased 2 and 6 h p.i., suggesting that a replication-dependent increase of DI RNA proceeds after the uptake of virion. The IFN induction and the level of DI RNA were almost parallel (Fig. 5, *A* vs *B*).

MV induces IFN via IKKε, TBK-1, and NAK-associated protein 1 (NAP1), but not TICAM-1

mDCs express TLR3 in the endosomes (39) and RIG-I/MDA5 in the cytoplasm (9, 10), which recognize dsRNA. TLR3 recruits TICAM-1/TRIF (29, 40) while RIG-I and MDA5 recruit MAVS/IPS-1/Cardif/VISA adaptors (31, 41–43). They converged upon NAP1, which assembles IKKε and TBK1 to follow the IRF-3-dependnet IFN-β-inducing pathway (28). Gene-silencing analysis was performed to identify the molecules that are involved in MV (ED)-mediated type I IFN induction.

HeLa cells expressing TLR3 responded to poly I:C to induce IFN-β (Fig. 6*A*, *right panel*). The mRNAs of TICAM-1, IKKε, and TBK1 were silenced with siRNA in this study. The gene-silenced cells were infected with MV ED and, 24 h later, the IFN-β mRNA levels were measured with the ED-infected cells. Cells depleted of IKKε or TBK1 hampered the high induction of IFN-β mRNA (Fig. 6*A*, *left panel*), suggesting that the two kinases are crucial factors for IFN-β induction. In contrast, the absence of TICAM-1 barely affected the ED-derived IFN-β mRNA level (Fig. 6*A*, *left panel*). Cells stimulated with poly I:C were used as control for the TLR3 pathway and, as expected, poly I:C-dependent IFN-β induction depended on TICAM-1, IKKε, and TBK1 (Fig. 6*A*, *right panel*). Likewise, NAP1 knockdown exhibited down-regulation of the IFN-β mRNA (Fig. 6*B*) when cells with stably silenced NAP1 or GFP were used instead of the transient knockdown cells (28). When NAP1-depleted cells were stimulated with poly I:C, 40% of the mRNA level was reduced within 6 h (cells die during long-term incubation with poly I:C). In the HeLa cell system, ED infection resulted in a 50% decrease of the NAP1-associated IFN-β induction. The incomplete blockade of IFN-β induction by NAP1 silencing may reflect the presence of an escaping NAP1 moiety due to a high endogenous level of NAP1 or functional compensation of NAP1 with other TANK family proteins (28, 44). Thus, MV ED induces IFN-β in HeLa cells, which involves NAP1, IKKε, and TBK1, but not TICAM-1. Therefore, the trigger for type I IFN induction by DI RNA is not the TLR3-TICAM-1 pathway.

Both RIG-I and MDA5 sense DI RNA

To determine whether RIG-I and/or MDA5 recognize DI RNA, we transfected the MV minireplicon RNA into HEK293/pISRE-luc cells (Fig. 3*B*) subtly overexpressing RIG-I or MDA5. ISRE promoter activation was 12-~18-fold increased due to the minimal constitutive expression of RIG-1or MDA5 (*left control bars* in Fig. 7). When DI RNA was added into the cytoplasm, high ISRE promoter activation was induced in these cells (Fig. 7). DI RNA was heated to denature the stem-loop structure or treated with CIAP to remove 5′ phosphates. In RIG-I-expressing cells, CIAP treatment of DI RNA more significantly reduced RIG-I-mediated IFN promoter activation than heat denaturation. In contrast, the reverse is true in MDA5-expressing cells, where CIAP treatment had almost no effect on MDA5-mediated IFN promoter activation. Hence, DI RNA enhances both RIG-I- and MDA5-mediated IFN-β induction. Both sense the stem-loop structure, while only RIG-I senses 5′ phosphates under the conditions setting.

DI RNA stimulates the cytoplasmic IFN-inducing pathway

We finally examined whether DI RNAs of MV follows the pathway involving RIG-I/MDA5 and MAVS for signaling IFN-β induction by gene-silencing technology. RIG-I, MDA5, MAVS, and TICAM-1 were silenced with siRNA (Fig. 8*A*), then MV minireplicon RNA or poly I:C was transfected into HeLa cells. Six hours later, the IFN-β mRNA levels were measured by Q-PCR (Fig. 8*B*). The siRNA of GFP was used as control. When MV minireplicon RNA was transfected into HeLa cells, the IFN-β mRNA levels in